



THE UNIVERSITY *of* EDINBURGH

Edinburgh Research Explorer

## Post-fire behaviour of continuous reinforced concrete slabs under different fire conditions

**Citation for published version:**

Wang, Y, Jiang, Y, Huang, Z, Li, L, Huang, Y, Zhang, Y, Zhang, G, Zhang, X & Duan, Y 2021, 'Post-fire behaviour of continuous reinforced concrete slabs under different fire conditions', *Engineering Structures*, vol. 226, 111342. <https://doi.org/10.1016/j.engstruct.2020.111342>

**Digital Object Identifier (DOI):**

[10.1016/j.engstruct.2020.111342](https://doi.org/10.1016/j.engstruct.2020.111342)

**Link:**

[Link to publication record in Edinburgh Research Explorer](#)

**Document Version:**

Peer reviewed version

**Published In:**

Engineering Structures

**General rights**

Copyright for the publications made accessible via the Edinburgh Research Explorer is retained by the author(s) and / or other copyright owners and it is a condition of accessing these publications that users recognise and abide by the legal requirements associated with these rights.

**Take down policy**

The University of Edinburgh has made every reasonable effort to ensure that Edinburgh Research Explorer content complies with UK legislation. If you believe that the public display of this file breaches copyright please contact [openaccess@ed.ac.uk](mailto:openaccess@ed.ac.uk) providing details, and we will remove access to the work immediately and investigate your claim.



# 1 **Post-fire behaviour of continuous reinforced concrete slabs under** 2 **different fire conditions**

3 Yong Wang <sup>a</sup>, Yaqiang Jiang <sup>a</sup>, Zhaohui Huang <sup>b,\*</sup>, Lingzhi Li <sup>a,c</sup>, Yun'er Huang <sup>d</sup>,  
4 Yajun Zhang <sup>a</sup>, Gengyuan Zhang <sup>e</sup>, Xiaoyue Zhang <sup>a</sup>, Yakun Duan <sup>a</sup>

5 <sup>a</sup> *State Key Laboratory for Geomechanics & Deep Underground Engineering, China University of Mining & Technology,*  
6 *Xuzhou, Jiangsu, 221116, China;*

7 <sup>b</sup> *Department of Civil and Environmental Engineering, Brunel University London, Uxbridge, UB8 3PH, UK*

8 <sup>c</sup> *College of Civil Engineering, Tongji University, 1239 Siping Road, Shanghai 200092, China*

9 <sup>d</sup> *School of Engineering, The University of Edinburgh, Edinburgh, UK*

10 <sup>e</sup> *China Academy of Building Research, Beijing 100013, China*

11 **Abstract:** An experimental investigation of the performance of reinforced concrete  
12 continuous slabs is presented in this paper, following the exposure of the slabs to different  
13 compartment fires. The influence that several factors, including compartment fire scenarios,  
14 reinforcement ratio, and bar arrangement, have on the deflections, strains, crack patterns, and  
15 failure modes is analysed. Results that compared to the uniform fire case, localized or  
16 extended punching shear failure modes are more likely to occur in the fire-damaged slabs  
17 subjected to the traveling fire due to more cracks. The residual structural stiffness and  
18 ultimate loads are enhanced with the increasing reinforcing ratio, but the brittle punching  
19 failure readily appeared. Finally, the deflection failure criterion ( $l/50$ ) and the ACI 318-08  
20 punching shear theory are helpful in predicting the residual ultimate loads of the fire-damaged  
21 slabs subjected to any fire scenario.

22 **Keywords:** continuous slab; post fire; failure mode; punching shear; ultimate load;  
23 theoretical analysis.

24  
25 \* Corresponding author, E-mail address: [zhaohui.huang@brunel.ac.uk](mailto:zhaohui.huang@brunel.ac.uk) ([Z. Huang](#))

## 28 **1. Introduction**

29 In recent years, the structural performance of reinforced concrete (RC) slabs in fire has  
30 received significant research attention. There have been numerous experimental and  
31 numerical studies on the fire performance of RC slabs [1-11]. However, there are limited  
32 studies on the residual load capacity of RC slabs to assess the extent of fire damage and  
33 reusability [12-14].

34 So far, the residual responses of isolated simply-supported concrete slabs have been primarily  
35 investigated. For instance, Chung et al. [15] investigated the residual strength of fire-damaged  
36 RC slabs by means of experimental tests and numerical simulations. However, the test  
37 specimens were not loaded during the fire, thus, the load capacities obtained from the test  
38 program did not agree with the real conditions of RC slabs in buildings. Wang et al. [16]  
39 conducted a test to investigate the residual strength of one full-scale fire-damaged RC two-  
40 way slab and proposed the reinforcement strain difference method to predict its load-  
41 deflection curve. It was found that the proposed method can be employed to determine the  
42 residual strength of post-fire simply supported two-way RC slabs. Apart from the isolated  
43 concrete slabs, several researchers conducted the tests on the residual structural performance  
44 of continuous slabs reinforced with either steel bars or GFRP bars after fire. For instance, Yu  
45 [17] investigated the residual capacity of five two-span continuous concrete slabs ( $5200 \times$   
46  $1200 \times 120$  mm) after exposed to fire. As expected, the residual bearing capacity and the  
47 initial structural stiffness gradually decreased as the heating time increased. Hou and Zheng  
48 [18] and Zheng et al. [19] investigated the post-fire mechanical performance of unbonded  
49 prestressed concrete (PC) continuous slabs. It was found that the degradation rate of the load-  
50 bearing capacity of PC slabs increased with the increase in heating time and load level.  
51 Meanwhile, Hajiloo and Green [12], Gao et al. [20] and Gooranorimi et al. [21] investigated  
52 the residual strength of fire-exposed GFRP-RC slabs. Contrary to RC slabs, GFRP-reinforced  
53 slabs frequently undergo bond-related failures.

54 The above review of literature shows that studies on the residual properties of concrete slabs  
55 subject to uniform fire have been extensively conducted, but less experimental data is

56 available on the residual properties of continuous slabs after exposed to different  
57 compartment fires. This is an important shortcoming of the available literature data, as  
58 different compartment fires frequently occur in modern buildings [22-25]. Thus, Wang et al.  
59 [26] investigated the post-fire residual behaviour of five continuous reinforced concrete slabs  
60 (named Slabs S1-PF to S5-PF) under various fire scenarios in the spans. The results indicate  
61 that the residual material properties of heated compartments and concrete spalling  
62 significantly affect the ultimate load and failure mode of the fire-damaged continuous RC  
63 slabs. Apart from the flexural failure mode, the punching shear failure also occurred in the  
64 fire-damaged continuous slab, particularly in the span with considerable explosive concrete  
65 spalling. Note that, the five tested slabs has the same reinforcement arrangement. In addition,  
66 about 180 min of fire duration was used in the five tests, including single-compartment, two-  
67 compartment and three-compartment fires. In fact, for many fire events, fires were observed  
68 to spread from one compartment to another compartment in the same floor or different floors  
69 [27]. Thus, the residual behaviour of the continuous slabs subjected to different compartment  
70 fires is more representative than the cases where all spans in the continuous slabs are  
71 subjected to a uniform fire.

72 Apart from the experimental studies, the theoretical methods need to be developed to assess  
73 the residual strength of the fire-damaged concrete slabs, particularly the residual bearing  
74 capacity and failure criteria [26]. At present, several theoretical methods [3, 16, 28-34] were  
75 developed to predict the bearing capacity of simply supported two-way concrete slabs at  
76 ambient and elevated temperatures. In those developed methods, different flexural failure  
77 modes were proposed to predict the bearing capacities of concrete slabs at large deflections  
78 (considering tensile membrane action). However, for fire-damaged concrete slabs, another  
79 failure mode, such as the punching shear failure, should be considered because of the material  
80 strength degradation and the decreased thickness of slabs resulted from concrete spalling [26].  
81 Therefore, the main objectives of this paper are: (1) to investigate experimentally the residual  
82 carrying capacity and failure mode of the each span of four three-span full-scale continuous  
83 RC slabs under various compartment fire scenarios as well as compare with the observations  
84 from other literature; (2) to establish the reasonable failure criteria to determine the residual

85 ultimate loads of the fire-damaged continuous slabs; (3) to apply the flexural and punching  
86 shear theories for evaluating the residual bearing capacity of the slabs and verify their  
87 effectiveness.

## 88 **2. Experimental program**

### 89 *2.1 Design of the specimens*

90 Four three-span RC continuous slabs (named Slabs B1 to B4) were designed according to the  
91 specifications of Chinese Standard GB50010-2010 [35]. All slabs were casted using  
92 commercial concrete with the characteristic cube strength of 30 MPa at the age of 28 days.  
93 The measured concrete cubic strength was 31.5 MPa. The age of the concrete at the time of  
94 fire testing was: Slab B1 = 749 days; Slab B2 = 701 days; Slab B3 = 716 days and Slab B4 =  
95 730 days, and the moisture content was 2.3%.

96 For each slab, hot-rolled reinforcing bars with a diameter of 8 mm were used, and the clear  
97 concrete cover was 15 mm. The average yield and ultimate strength of the reinforcing steel  
98 were 414 MPa and 475 MPa at ambient temperature, respectively. Figs. 1(a) and 1(b) shows  
99 the details of steel reinforcement layouts of the four slabs.

### 100 *2.2. Test procedure*

#### 101 *2.2.1 Fire tests*

102 For the four fire tests, the variables included the reinforcement ratio (spacing: 100 mm or 200  
103 mm), reinforcement layout (discontinuous or continuous on the top reinforcement layout),  
104 and different compartment fires. According to Chinese design code [36], the fire resistance  
105 of a building is classified as Classes 1 to 4. In fact, to avoid the rapid fire spreading within a  
106 building, the fire compartment wall is required. For the fire compartment walls, the required  
107 fire resistance times for Classes 1 to 4 buildings are 15 min, 30 min, 45 min and 60 min,  
108 respectively. Note that, for the residential building, the fire resistance of the fire compartment  
109 wall is at least 30 min. In this case, two time delays (30 min and 60 min) were used to  
110 represent the fire spreading from one compartment to another. The fire test durations of four  
111 slabs (Slabs B1 to B4) were 360 min, 400 min, 600 min and 600 min, respectively.

112 During the fire test, each slab was continuous over the interior support (refractory pellet) and  
113 was simply-supported on steel rollers at the exterior supports, and each corner was held down  
114 by a steel beam. In addition, the uniform distribution load ( $2.0 \text{ kN/m}^2$ ) on the top surface of  
115 the slab was applied using iron brick.

116 The locations of three fire compartments A, B, and C are shown in Fig. 1(a). For Slab B1: At  
117 0 min, Compartment B was firstly exposed to fire, and at 60 min, Compartments A and C  
118 were simultaneously exposed to fire. At 180 min (235 min), the nozzles in all three  
119 Compartments were shut off. For Slab B2: The sequence of the three compartment fires was  
120 similar to that of Slab B1, but the time interval between Compartment B and Compartments  
121 A and C was 30 min. For Slab B3: Compartments A, B, C were sequentially exposed to fire,  
122 and time delay was 60 min. For Slab B4: Compartments A, C, B were sequentially exposed  
123 to fire, and the time interval and the fire duration of each compartment were 60 min and 180  
124 min, respectively. Note that, for each compartment, its heating time was about 180 min.

125 Locations of thermocouples are indicated in Figs. 1(c) and 1(d), and other details of four fire  
126 tests can be found in Ref. [27].

### 127 **2.2.2 Residual tests**

128 After the fire tests all four slabs were moved from the furnace and stored in the structural lab  
129 for approximately 3 months. Then the fire-damaged slabs were tested on the new test rig, as  
130 shown in Fig. 2. For the residual tests, the fire-damaged slabs were renamed as Slabs B1-PF  
131 to B4-PF for Slabs B1 to B4.

#### 132 (1) *Loading apparatus*

133 As shown in Figs. 2(a)-2(b), based on the Standard of Concrete Testing Method of China [37],  
134 the slab's edges were simply supported by steel rollers on the wall, and the load was applied  
135 to the slab using two jacks. There were no horizontal restraints provided along the edges of  
136 the slab.

137 For the residual tests, the loading was applied proportionally on the three spans. Before the  
138 load reached 150 kN, at each loading step, the load increment on each span was 30 kN. In  
139 other words, the load increment on Jack J1 was 30 kN, and that on Jack J2 was 60 kN. The

140 load on each compartment applied by Jack J2 can be obtained according to the corresponding  
141 pressure transducer (see Fig. 2(c)). After the load reached 150 kN, the load increment on each  
142 span was 10 kN. The applied load at each loading step was kept for 5 min.

143 As indicated in Fig. 2(c), each corner of the slab was held down by a steel beam. The reaction  
144 forces at the corners were measured by four pressure transducers (Points P-1 to P-4). The  
145 failure of a slab was governed by: 1) conventional mid-span deflection failure criterion; 2)  
146 concrete crushing on the top surface; and 3) punching shear failure. Once any one of those  
147 failure conditions was reached, the test was terminated.

#### 148 (2) *Strain measurement*

149 Concrete strain gauges (such as Points A-C-1 and A-C-2) were placed on the top surface of  
150 the slabs, as shown in Fig. 3(a). To reduce the damage of the test slabs, only four bottom  
151 reinforcement strain gauges (such as Points A-S-1 to A-S-4) were arranged in each span of  
152 the slabs.

#### 153 (3) *Deflection measurement*

154 Fig. 3(b) shows the positions of the vertical and horizontal displacement transducers. Three  
155 LVDTs (Points V-A, V-B, and V-C) were placed to measure the mid-span vertical deflections  
156 of the slab, while its horizontal deflections were measured by two LVDTs (Points H-1 and H-  
157 2).

### 158 **3. *Fire test results***

159 Figs. 4 and 5 show the average furnace temperature, concrete and steel temperature-time  
160 curves of four slabs during the fire test. Table 1 gives the maximum temperatures of each  
161 compartment, concrete (top and bottom surfaces) and steel (bottom and top steel) at various  
162 locations in Slabs B1 to B4. As indicated in Fig. 1(d), for concrete, each thermocouple tree  
163 consisted of six thermocouples (such as AT-1 to AT-6) and for steel reinforcement, there were  
164 four thermocouples (such as R-1 to R-4).

165 As indicated in the Table 1, the maximum temperatures for the bottom concrete (steel) ranged  
166 from 671 (529) °C to 1130 (718) °C, with an average value of 893 (645) °C. The residual  
167 strength of the bottom concrete and the bond between concrete and steel were seriously

168 damaged due to the higher temperatures. In contrast, the top concrete and the bond between  
169 concrete and steel had higher residual strengths due to the lower maximum experienced  
170 temperature (average value: 246 °C and 345 °C). As discussed in Ref. [26], the average  
171 concrete (steel) temperatures on the bottom and top surfaces of the heated spans were 828  
172 (781) °C and 254 (497) °C, respectively. Note that, as indicated in Fig.4, the maximum  
173 temperatures near to top surface of each span reached after the time of maximum gas  
174 temperature. The delayed failure (structural integrity) of each span occurred during the  
175 cooling phase, although the most spans exhibited integrity during the heating phase. In fact,  
176 as discussed in Refs. [38-39], more attentions should be brought to the structural behaviour  
177 during the cooling phase, and thus the duration of heating phase (DHP), was proposed to  
178 assess the burnout resistance of the member throughout a given fire exposure.

179 Similar to the observations in Ref. [26], severe post-cooling spallings (with the concrete  
180 falling into pieces) occurred prior to the residual test due to the moisture absorbed by the  
181 calcareous aggregate (rehydration). Compared to thermal-hygral or thermal-mechanical  
182 spalling [40], the post-cooling spalling was much slower, but it continued up to the beginning  
183 of the residual test (approximately 2 months). This post-cooling spalling should be considered  
184 in the repair, since the bottom weak concrete layer will seriously affect the bond strength  
185 between concrete and steel. In addition, it can be seen from Table 1 that the residual  
186 deflections of each span for Slabs B1 to B4 at the end of the fire test were relatively small.  
187 However, for the large deformed slab during fire test the residual performance of that slab  
188 may be different compared to the the present slabs due to various permanent and irrecoverable  
189 strains, such as the plastic and transient creep strains [38-39].

#### 190 *4. Post-fire mechanical tests*

191 This section discusses the residual behaviour of each slab and a brief explanation of the  
192 observed behaviours, including the new cracks, failure mode, load-deflection curves, reaction  
193 forces at the corners, and the concrete and steel strains.

##### 194 *4.1 Failure behaviour*

195 Figs. 6–9 show the crack pattern and spalling on the top and bottom surfaces of each span in



196 the four slabs. For each fire-damaged slab, the red and dark lines indicate new and original  
197 cracks which were formed during the fire test, respectively.

#### 198 **4.1.1 Crack patterns**

##### 199 ● Slab B1-PF

200 Figs. 6(a) and (b) show the crack pattern on the top surface of slab B1-PF (steel spacing: 200  
201 mm). During the residual test, before the loading reached 120 kN, small new cracks appeared  
202 on the top surface, and the original cracks gradually widened with increasing loads. After 120  
203 kN, large new arc cracks appeared near the four corners of each span. Due to the higher strain  
204 on the concrete corners ( $2672 \mu\epsilon$ ), the concrete crushing occurred on the top surface of Span  
205 A. In addition, for Span B, one circular punching cone (red circle) formed in the middle region,  
206 indicating that the shear punching failure (shear-compression crush: a combination effect of  
207 both shear and compression forces) occurred in this span. However, for Span C, only arc  
208 cracks appeared on the top surface, and no brittle failure occurred.

209 Figs. 6(c) and (d) show the crack pattern on the bottom surface of Slab B1-PF. Clearly, there  
210 were two kinds of failure modes, i.e., the flexural failure mode (Spans A and C) and the  
211 overall punching failure mode (Span B). For Spans A and C, the flexural cracks extended  
212 from the centre to the edges, while the shear punching area appeared at the centre of Span B.  
213 The main reason is that there were numerous original cross cracks (+ shape) on the top surface  
214 of Span B, and fewer cross cracks appeared on the two edge spans. The original cross cracks  
215 appeared owing to the upward deflections (or negative moments) of Span B during the fire  
216 [27], and the crack spacing basically coincided with the steel spacing (200 mm) [16, 41].  
217 Clearly, these cracks led to a serious degradation of the structural integrity, decreased bond,  
218 and the stress (strain) concentration. For instance, as discussed later, the steel at three points  
219 of Span B suddenly exceeded  $10000 \mu\epsilon$  at approximately 160 kN, indicating that a brittle  
220 failure and strain concentration occurred. The comparison implies that the original cracks that  
221 occurred during the fire test had important effects on the failure modes of the fire-damaged  
222 slabs.

##### 223 ● Slab B2-PF

224 Figs. 7(a) and (b) show the crack patterns on the top surface of Slab B2-PF (steel spacing:  
225 200 mm). During the residual test, before the loading reached 60 kN, many small arc cracks  
226 appeared on the top surface of Spans A and C. As the load increased, the arc cracks gradually  
227 widened. At approximately 210 kN, a punching shear failure of Span C occurred with one  
228 hole. Furthermore, the concrete crushing (maximum concrete strain: 3386  $\mu\epsilon$ ) on the top  
229 surface of Span A suddenly occurred as well as the steel yielding (reinforcement strain:  
230 exceeded 10000  $\mu\epsilon$ ), as discussed later. Thus, compared to Slab B1-PF, the structural stiffness  
231 of Slab B2-PF was larger, owing to the shorter fire duration and fewer original cross cracks  
232 (smaller fire time delay, i.e., 30 min). This observation also implies that the fire scenarios  
233 have important effects on the failure mode of the middle span in the fire-damaged slab, as  
234 they can lead to different cracks or spalling during the heating stage [27].

235 Figs. 7(c) and (d) show the crack pattern on the bottom surface of Slab B2-PF. Clearly,  
236 compared to Span B, serious flexural-punching shear failure occurred in Spans A and C due  
237 to higher experienced temperatures (see Table 1) and lower boundary restraint, particularly  
238 on Span C.

239 Hence, the failure mode of each span in one continuous slab was primarily dependent on the  
240 experienced maximum temperatures, fire duration, equivalent reduction factor of the strength  
241 across the section, and original crack distribution. In addition, the comparison between Slabs  
242 B1-PF and B2-PF indicates that the time delays (30 min and 60 min) have an important effect  
243 on the failure mode of the initially heated span of the continuous slab. As the time delay  
244 increased, the possibility of punching shear failure increased, e.g. Span B1-PF-B.

245 ● Slabs B3-PF and B4-PF

246 Figs. 8(a) and (b) show the crack pattern on the top surface of Slab B3-PF (steel spacing: 100  
247 mm). Due to many small original cracks in Spans B and C, punching shear failure occurred  
248 with four holes on the top surface and smaller vertical deflections. These punching shear areas  
249 appeared around the loading plate on the top surface.

250 More importantly, in contrast to Slabs B1-PF and B2-PF, a large amount of concrete (area:  
251 2.5 m<sup>2</sup>) fell from the bottom surface of two spans in Slab B3-PF (Figs. 8(c) and (d)),  
252 particularly near the interior supports. The main reason for this is that higher reinforcement

253 ratio led to more small and tiny original cracks [27], indicating that the bond between the  
254 concrete and steel was seriously compromised. In addition, owing to fewer original cracks in  
255 Span A, the flexural failure modes occurred, such as new corner and arc cracks. Thus, the  
256 failure mode indicated that the fire-damaged slabs with higher reinforcement ratios had a  
257 higher residual bearing capacity, but the punching shear failure easily occurred because of  
258 numerous small original cracks (negative moment). Compared to Slabs B1-PF and B2-PF,  
259 the original crack width on the top surface of Slab B3-PF was much smaller due to the smaller  
260 steel spacing (100 mm). The comparison indicates that the residual property of the steel has  
261 a large effect on the flexural carrying capacities; however, the residual property of the  
262 concrete, original crack patterns (particularly crack spacing), and load type (concentrated load)  
263 have a greater effect on the failure mode.

264 Figs. 9(a) and (b) show the crack pattern on the top surface of Slab B4-PF (steel spacing: 200  
265 mm). In contrast to the flexural failure (arc and flexural cracks) of Spans A and B, the  
266 punching shear failure of Span C occurred. In addition, like Slabs S1-PF and S2-PF, the  
267 bottom concrete in Slab B4-PF did not fall off, as shown in Figs. 9(c) and (d). However, due  
268 to the negative reinforcement layout, the bearing capacity (120 kN) of Slab B4-PF was the  
269 smallest. The comparison further indicates that the reinforcement ratio and reinforcement  
270 layout have a significant effect on the bearing capacity of the fire-damaged slabs. Hence, the  
271 beneficial or detrimental effects of the reinforcement ratio (layout) should be considered in  
272 the residual property judgement of post-fire continuous slabs.

#### 273 **4.1.2 Failure criteria**

274 Table 2 shows the bearing capacity ( $P_u$ ) and ultimate deflection of each span ( $\delta_u$ ) in the four  
275 slabs at the end of the residual test. Note that, the post-fire failure of the slab is assumed to  
276 occur when [37]: (1) The concrete crushing occurs on the top surface of one span. (2) The  
277 mid-span deflection of one span exceeds  $l/50$ ,  $l$  is the length of the shorter span. (3) The  
278 punching inside or outside the shear zone occurs in any span.

279 To be conservative, the smallest load of three spans can be considered as the bearing capacity  
280 of the slabs. Thus, the bearing capacities of Slabs B1-PF to B4-PF were 145.3 kN, 190.4 kN,

281 229.1 kN, and 120.0 kN, respectively.

282 As shown in Table 2, for one span with yield failure, the ultimate deflections ranged from  
283 26.9 mm to 51.1 mm, with an average deflection of 37.5 mm. In addition, for the spans with  
284 punching shear failure, the ultimate deflections ranged from 14.9 mm to 34.5 mm, with the  
285 average ultimate deflection of 25.3 mm. Thus, for a post-fire slab with any failure, the  
286 deflection failure criterion  $l/50$  (about 29 mm) is suitable for determining the residual bearing  
287 capacity of the span. This observation is similar to the conclusion in Ref. [26].

288 In fact, the conventional reinforcement strain (such as 0.01) is often used to determine the  
289 bearing capacity of unheated slabs [35]. However, this is not suitable for determining the  
290 bearing capacity of the heated slabs. For instance, for many spans, the reinforcement strains  
291 at lower load levels exceeded  $10000 \mu\epsilon$  due to the combination of several factors, including  
292 load concentration, cover falling, decreased steel properties and bond degradation. As  
293 discussed later, a larger value of steel failure strain (0.02) may be more reasonable.

#### 294 ***4.1.3 Discussions***

295 According to the observation in Ref. [26] and the present slabs, it can be concluded that  
296 compared to Slabs S1-PF to S5-PF (exposed to uniform fire), the punching shear failure or  
297 the flexural-punching combined failure easily appeared in the present slabs subjected to  
298 traveling fire. For instance, only four spans in Slabs S1-PF to S5-PF (total 15 spans) had the  
299 punching shear failure, but six spans in Slabs B1-PF to B4-PF (total 12 spans) showed this  
300 failure behaviour. One reason is the longer fire duration of the present tested slabs. Another  
301 reason is that more cross shape (+) original cracks and long-span cracks appeared on the top  
302 surface of Slabs B1 to B4 due to the complex deflection trend (upward and downward  
303 deflection) of each span [27]. No doubt, this cracking pattern led to the lower structural  
304 integrity of the fire-damaged slab and thus its flexural behaviour cannot sufficiently develop.  
305 On the other hand, for Slabs S1-PF to S5-PF [26], many short-span original cracks mainly  
306 appeared near to the internal supports, and thus the failure at internal support (larger cracks  
307 on the top surface) easily appeared during their residual tests. However, for the present tested  
308 slabs, less failure at internal support appeared and larger cracks mainly appeared on the

309 middle region of each span.

310 In all, the above comparison indicates that the fire scenarios (uniform and travelling fire) have  
311 important effect on the failure mode of the fire-damaged continuous slabs, since they led to  
312 different original cracking distribution of the slabs during the fire test. In other words, for the  
313 uniform fire case, the slab over internal supports may be the weakest region of the continuous  
314 slab. For the travelling fire case, the mid-span region of each span may be the weakest region  
315 of the slab. No doubt, this observation should be further verified by more residual strength  
316 tests of the continuous slabs.

317 Note that, because of the concentrated loads, punching shear failure at the loading location is  
318 a recurring event. Thus, the loading system considerably influences the failure mode of the  
319 fire-damaged slabs, and the present observation may not suitable for the uniform load case.  
320 However, the present loading case can be considered as the worst case. In fact, for most  
321 practical design cases, the brittle punching shear is undesirable, the yield mechanism cannot  
322 develop before punching. Thus, one traveling fire scenario which easily leads to the punching  
323 shear failure of the fire-damaged slab, particularly near to the support, can be considered as  
324 the worst fire scenario. In addition, for the post-fire rehabilitation and resilience, the  
325 reasonable strengthening technique should be used to change the mode of failure from  
326 punching shear failure to a pure flexural failure [42-44], including the cementitious materials  
327 (ECC or epoxy matrix), installation method (prefabricated or cast-in-place), reinforcement  
328 type (FRP, reinforcing bar and steel plate).

## 329 ***4.2 Deflection and corner forces***

330 This section discusses the vertical and horizontal deflections of each slab as well as the  
331 reaction forces at the corners. For the vertical deflection, positive (negative) displacement is  
332 downward (upward); while for the horizontal deflection, positive (negative) displacement  
333 indicates outward (inward) movement.

### 334 ***4.2.1 Load-mid-span vertical deflection response***

335 Figs. 10(a)–(d) show the load-deflection curves of the fire-damaged Slabs B1-PF to B4-PF.  
336 In addition, the initial residual structural stiffness ( $K_0$ ), the residual bearing capacities ( $P_u$ ),

337 energy ductility ( $\mu_E$ ) and the ultimate deflections ( $\delta_u$ ) are briefly discussed, as indicated in  
338 Table 2. Note that, the initial structural stiffness  $K_0$  of each span is the ratio between  $P_e$  and  
339 its corresponding mid-span deflection ( $\delta_e$ ), and  $P_e$  and  $\delta_e$  values of each span can be obtained  
340 according to the significant variation in the slope of the load-deflection curves.

#### 341 ● Initial residual structural stiffness

342 As shown in Table 2, for the four fire-damaged slabs, the average  $K_0$  of the middle and edge  
343 spans were 8.6 and 15.3 kN/m, respectively. This is similar to the average values (13.03 kN/m)  
344 of the heated spans in Ref. [26]. However, for Slabs S1-PF to S5-PF, there are larger difference  
345 among  $K_0$  due to different number and position of the heated spans. For the present slabs, the  
346 difference in the initial structural stiffness between the middle span and the edge span can be  
347 neglected, as indicated in Table 2. Thus, the beneficial effect of the boundary restraint can be  
348 neglected in the residual serviceability assessment, particularly for exposed to travelling fire  
349 case.

#### 350 ● Energy absorption

351 The energy ductility ( $\mu_E$ ) was used to assess the ductility, as shown in Table 2 and Fig. 11.  
352 The energy ductility ( $\mu_E$ ) is  $(E_{total}/(2E_{el}) + 0.5)$ , where  $E_{total}$  and  $E_{el}$  are the elastic and total  
353 energies (areas of the load-deflection curve) of the fire-damaged slab [20, 26], respectively.  
354 As shown in Table 2, the  $\mu_E$  value of the heated middle (edge) spans ranged from 1.06 (1.26)  
355 kN mm to 1.90 (4.80) kN mm, with the average value of 1.32 (2.55) kN mm. Note that, this  
356 observation is different from those of the concrete slabs (thickness: 80 mm) subjected to  
357 uniform fire [26]. For instance, the  $\mu_E$  value in Ref. [26] of the heated middle (edge) spans  
358 ranged from 9.99 (1.58) kN mm to 19.91 (6.28) kN mm, with the average value of 13.38  
359 (3.22) kN mm. On one hand,  $\mu_E$  of the present slabs (thickness: 100 mm) were smaller than  
360 those of the tested slabs in Ref. [26]. As the depth increased, the ductility was decreased. On  
361 the other hand, there were smaller fluctuations in the  $\mu_E$  values of the present concrete slabs,  
362 particularly in those of the middle spans, indicating that the effect of the boundary restraint  
363 on  $\mu_E$  decreased. Thus, compared to uniform fire scenario, the traveling fire scenario tends to  
364 decrease the residual structural ductility of the concrete slab due to more complex cross cracks  
365 and longer fire duration. In all, the effect of the fire scenario (uniform or traveling) on the

366 residual structural behaviour should be considered in the post-fire performance assessment or  
367 repair design.

368 ● **Bearing capacity**

369 For each slab, the minimum ultimate load within the three spans was considered as the actual  
370 ultimate load of the slab. Thus, the bearing capacity of Slabs B1-PF to B4-PF were 145.3 kN,  
371 190.4 kN, 229.1 kN, and 120.0 kN, respectively, with an average value of 171.2 kN. Due to  
372 larger thickness (100 mm), the ultimate load of the present tested slabs were relatively higher  
373 than those (average value: 126.8 kN) of Slabs S1-PF to S5-PF (thickness: 80 mm) [26]. In  
374 addition, compared to the other three fire-damaged slabs, the bearing capacity of Slab B4-PF  
375 was the minimum due to the smaller reinforcement ratio, discontinuous top reinforcement  
376 layout, and longer fire duration. Thus, continuous reinforcement layouts and higher  
377 reinforcement ratios are beneficial to enhance the residual carrying capacities of the slabs  
378 (Slab B3-PF), particularly the flexural capacities, as the flexural strength is mainly dependent  
379 on the reinforcement strength and concrete compressive strength on the top surface [45-46].

380 It can be seen that for any fire scenario, increasing thickness and reinforcement ratio are the  
381 most effective methods to enhance the residual capacities of the continuous slabs. However,  
382 the possibility of punching shear (brittle or sudden) failure increases with increasing  
383 reinforcement ratio due to the smaller crack spacing.

384 Overall, for any fire scenario, the ultimate load of one span in the fire-damaged continuous  
385 slab was primarily dependent on the reinforcement ratio and layout, original crack distribution,  
386 cover falling, and boundary conditions. Increasing the reinforcement ratio, providing a  
387 continuous reinforcement layout, increasing the original crack spacing and strengthening the  
388 cover will be beneficial to enhancing the residual strength of the fire-damaged slabs. In  
389 addition, different compartment fires (different fire directions or time delays) that lead to  
390 more original cracks and serious concrete spalling in one span will result in a decreased  
391 residual strength or brittle failure, particularly in the middle span.

392 **4.2.2 Horizontal deflection and reaction forces**

393 Fig. 12(a) shows the measured horizontal deflection-load curve of Slabs B1-PF and B2-PF.

394 The horizontal deflection is the horizontal component of the corresponding local  
395 displacement. During the early stage, the horizontal deflection of each measured point was  
396 small due to the small vertical deflection. As the load increased, the horizontal deflection  
397 rapidly increased until the end of the test, particularly for Point H-2. In addition, the load-  
398 deflection trends differed between Points B1-PF-H-1 (B2-PF-H-1) and B1-PF-H-2 (B2-PF-  
399 H-2). However, compared to the maximum vertical deflections, the maximum horizontal  
400 deflection (approximately 3 mm) of each post-fire slab was smaller. In all, the deflection trend  
401 and the maximum horizontal deflection were similar to the observation in Ref. [26].

402 Figs. 12(b)-(c) show the reaction forces measured by pressure sensors P-1 to P-4 of Slabs B1-  
403 PF and B3-PF. On the one hand, similar to the results in Ref. [26], the reaction forces at each  
404 measured point gradually increased with increasing loads, and the maximum values were 11.0  
405 kN and 14.0 kN, respectively. On the other hand, at the end of each test, the average reaction  
406 forces at the four points were 8.1 kN and 10.1 kN, respectively. It can be seen that the fire  
407 scenario has little effect on the residual horizontal deflection and the reaction forces of the  
408 fire-damaged continuous slabs.

#### 409 ***4.3 Concrete and reinforcement strains***

410 The measured concrete and reinforcement strains for the slabs are shown in Figs. 13(a)-(d),  
411 and the concrete peak strain and steel yield strain are given according to Ref. [45]. A positive  
412 value represents a tension strain while a negative value indicates a compressive strain. The  
413 strains at some measured points are not shown, owing to the malfunction of the strain gauges.  
414 As shown in Figs. 13(a)-(d), during the early stage, the concrete strain at each point was small.  
415 Then, the concrete compressive strain at each corner quickly increased with the load until the  
416 end of the test. In addition, in some cases, concrete crushing occurred during the test, such as  
417 with Spans B1-PF-A and B2-PF-A, and the measured concrete strains nearly reached the peak  
418 strains. However, for the punching shear failure mode, the measured concrete strain was  
419 smaller, such as with Span B3-PF-C. For instance, the average maximum concrete strains  
420 were  $2409 \times 10^{-6}$  (Span B1-PF-A: 180 kN),  $2701 \times 10^{-6}$  (Span B2-PF-A: 209 kN) and  $671 \times$   
421  $10^{-6}$  (Span B3-PF-C: 227 kN), respectively. Thus, similar to the observation in Ref. [26], the



422 corner concrete strain can reflect the failure mode of the post-fire continuous slab.  
 423 As indicated in Figs. 13(a)–(d), the reinforcement strains in most of the measured points  
 424 gradually increased with the loads; however, similar to the reinforcement strain development  
 425 in Slabs S1-PF to S5-PF [26], there were remarkable differences between the measured points  
 426 in one span of the slab. More importantly, at lower loads, the reinforcement strains of some  
 427 measured points were larger than 10000  $\mu\epsilon$ , but the post-fire slabs had higher carrying  
 428 capacities (such as Spans B2-PF-A and B3-PF-A). For instance, the reinforcement strains  
 429 observed were far higher than the yield strains, particularly for Points A (B and C)-S2. The  
 430 main reason is that the spalling did not occur uniformly, resulting in an inconsistent stress or  
 431 strain distribution, particularly near the loading plate. On the other hand, the concrete cover  
 432 basically lost all of its strength, and the stress cannot effectively be transferred between  
 433 concrete and steel. Thus, the serious bond degradation led to the concentrated or local damage  
 434 during the residual test. It can be concluded that the conventional reinforcement strain failure  
 435 criterion (such as 0.01) was not suitable for determining the residual bearing capacity of the  
 436 post-fire slab; otherwise, the ultimate loads may be seriously underestimated.

### 437 *5. Theoretical analysis*

438 In this section, several models (flexural and punching shear theories) were used to assess their  
 439 applicability in the prediction of the residual load capacities of the slabs. The residual  
 440 properties of concrete and steel were determined based on Ref. [47], as shown in Table 3. In  
 441 addition, the equivalent concrete residual tensile and compressive strengths across the  
 442 thickness were calculated according to Ref. [48], and they can be given by

$$f_{cu,T}^* = \bar{\varphi}_{c,T} f_{cu,20}, \quad f_{t,T}^* = \bar{\varphi}_{t,T} f_{t,20} \quad (1)$$

$$\bar{\varphi}_{c,T} = \frac{\sum_{i=1}^n \bar{\varphi}_{c,T_i} \cdot h_i}{h}, \quad \bar{\varphi}_{t,T} = \frac{\sum_{i=1}^n \bar{\varphi}_{t,T_i} \cdot h_i}{h} \quad (2)$$

$$\bar{\varphi}_{c,T_i} = 1 - 5.71 \times 10^{-4} T_i + 6.34 \times 10^{-7} T_i^2 - 3.42 \times 10^{-9} T_i^3 + 2.44 \times 10^{-12} T_i^4 \quad (3)$$

$$\bar{\varphi}_{t,T_i} = 1 - 7.29 \times 10^{-4} T_i - 1.38 \times 10^{-6} T_i^2 + 1.18 \times 10^{-9} T_i^3 - 1.23 \times 10^{-14} T_i^4 \quad (4)$$

443 where  $\bar{\varphi}_{t,T}$  and  $\bar{\varphi}_{c,T}$  are the equivalent residual tensile and compressive strength factor,

444 respectively;  $\bar{\varphi}_{c,T_i}$  ( $\bar{\varphi}_{t,T_i}$ ) is the  $i$ th layer concrete compressive (tensile) strength reduction  
445 factor at  $T_i$  [45];  $T_i$  is the maximum experienced temperature at  $i$ th layer;  $h$  is the slab thickness;  
446  $h_i$  is the thickness of  $i$ th layer;  $n$  is the number of the layers;  $f_{t,T}^*$  and  $f_{cu,T}^*$  are the equivalent  
447 residual tensile and compressive concrete strength across the section, respectively;  $f_{t,20}$  and  
448  $f_{cu,20}$  are the tensile and compressive strength at ambient temperature, respectively.

## 449 **5.1 Theoretical methods**

450 Theoretical methods included the yield line method [9], membrane action methods [3-4, 7],  
451 reinforcement strain difference method [16], and punching shear methods [35, 45-46]. The  
452 application of these membrane methods is limited to simply supported slabs at large  
453 deflections. Thus, their application or effectiveness is verified by the present fire-damaged  
454 continuous slabs subjected to the traveling fires.

### 455 5.1.1 Bailey method [3-4]

456 Bailey et al. [3-4] proposed a simple analytical method to determine the ultimate load-  
457 carrying capacity of two-way concrete slabs incorporating the tensile membrane action. The  
458 method was based on rigid-plastic behaviour with a change in geometry; the slab supports the  
459 load because of tensile membrane action in the central area of the slab and a ring of  
460 compressive membrane action around the perimeter. In this method, four enhancement factors  
461 ( $e_1 = e_{1m} + e_{1b}$  and  $e_2 = e_{2m} + e_{2b}$ ) for the load carrying capacities caused by the membrane and  
462 bending moment were proposed, and the overall enhancement for one slab is given by  
463  $e = e_1 - (e_1 - e_2) / (1 + 2\mu a^2)$ , as shown in Table 4. Finally, the deflection failure criterion was used  
464 to determine the enhancement factor ( $e$ ) of the slab. Other details can be found in Refs. [3-4].

### 465 5.1.2 Dong method [7]

466 Dong [7] presented a segment equilibrium method to determine the tensile membrane effects  
467 of concrete slabs, as shown in Table 4. This model mainly considers the tensile membrane  
468 action that is provided by the vertical component of reinforcement tensile forces after the  
469 formation of the mechanism of the plastic hinge line. The deflection failure criterion was  
470 proposed to determine the bearing capacity of RC slabs.

### 471 5.1.3 Reinforcement strain difference method [16]

472 The authors [16] proposed the reinforcement strain difference method to predict the residual  
473 loads of two-way fire-damaged slabs, as shown in Table 4. In the method, one two-way slab  
474 was divided into five parts, i.e., four rigid plates and the central rectangular (square) region.  
475 The reinforcement strain difference ( $\Delta\bar{\varepsilon}_{xx}$ ) of a slab is the average reinforcement strain  
476 difference between mid-span and the edge of the central rectangular region; it represents the  
477 degree of double curvature of the deformed slab. The relationship between the angle of the  
478 rigid plates ( $\theta_x$ ) and the reinforcement strain difference ( $\Delta\bar{\varepsilon}_{xx}$ ) was proposed to predict the  
479 ultimate loads or load-deflection curve of the slabs. In this study,  $\theta_x$  and  $\Delta\bar{\varepsilon}_{xx}$  are 0.15 and  
480  $1.0e-4$ , respectively.

### 481 5.1.4 Punching shear methods

482 The punching shear methods were given in the Chinese code [35], ACI318-08 code [45] and  
483 EN 1994-1-1 code [46], and their equations were summarized in Table 5.

## 484 **5.2 Theoretical results**

485 The comparison between the theoretical results and the experimental values are indicated in  
486 Table 6. For the yield line theory, the ratio ( $P_y/P_u$ ) ranged from 0.73 to 1.52, with an average  
487 value of 1.07 and a variation coefficient of 0.23. Clearly, the predicted ultimate load was not  
488 conservative, indicating that the yield line failure mode insufficiently developed in the present  
489 tested slabs, due to the strain or stress concentration. As discussed above, for the traveling  
490 fire case, the mid-span region of each span was the weakest region due to many original (+)  
491 cracks. In contrast, as discussed in Ref. [26], the ultimate load of each span predicted by the  
492 yield-line method was smaller than the experimental results. The comparison indicates that  
493 the yield line method is not suitable for predicting the ultimate loads of the fire-damaged  
494 continuous slabs subjected to the traveling fire, particularly many original cracks appeared in  
495 the mid-span region.

496 As expected, for other methods considering the tensile membrane action, the residual carrying  
497 capacities were overestimated. For instance, the average ratios  $P_b$  ( $P_d$  and  $P_s$ )/ $P_u$  were 1.36,  
498 1.37, and 1.25, respectively. This conclusion is different from the observation in Ref. [26].

499 Thus, for the present fire-damaged slabs subjected to traveling fire, the effect of the tensile  
500 membrane cannot be considered.

501 According to the punching shear failure (PSF) mode, the punching shear capacity of each  
502 span was predicted by Chinese code [35], ACI 318-08 code [45], and EC4 code [46], as  
503 indicated in Table 6. Their average ratios ( $P_p/P_u$ ) were 0.91 (Chinese code), 0.76 (EN code),  
504 and 0.83 (ACI 318-08), respectively. Clearly, compared to the flexural strength, the punching  
505 shear capacity of the fire-damaged slab seriously decreased. In addition, this difference is  
506 because different relationships between the concrete strength and the punching shear capacity  
507 were used in the three current codes, i.e., linear (Chinese code), 1/2 power (ACI 318-08), 1/3  
508 power (EN code). In all, according to Ref. [26] and the present results, it can be concluded  
509 that for any fire scenario, the punching shear capacity predicted by ACI 318-08 code was  
510 relatively reasonable.

## 511 **6. Conclusions**

512 This paper presents an experimental investigation on the residual properties of four  
513 continuous RC slabs after different compartment fires, and several theoretical methods were  
514 used to predict the ultimate load of each span in the present slabs. Meanwhile, the present  
515 results were mainly compared with the observation of the previous residual tested slabs  
516 subjected to uniform fire. Based on the above investigation, the following conclusions were  
517 drawn:

- 518 (1) Different from the continuous slabs subjected to the uniform fires, the punching shear  
519 failure or the flexural-punching failure mode more easily appeared in the tested slabs  
520 subjected to the traveling fires due to many original cross shape cracks in the middle  
521 region of each span.
- 522 (2) Compared to the fire spread direction and time delay, the reinforcement ratio,  
523 reinforcement arrangement and slab's thickness have more important effects on the  
524 residual ultimate loads of the fire-damaged continuous slabs.
- 525 (3) Different from the uniform fire case, the yield line method and the tensile membrane  
526 action method are not suitable for determining the residual ultimate loads of the

527 continuous slab subjected to the traveling fire scenario, since the yield line failure mode  
528 cannot sufficiently develop due to the strain or stress concentration.

529 (4) For any fire scenario, the deflection failure criterion ( $l/50$ ) and ACI 318-08 code can be  
530 used to determine the residual ultimate load of the fire-damaged continuous slab with  
531 lower span-thickness ratio.

### 532 **Acknowledgements**

533 This research was supported by the National Natural Science Foundation of China (Grant No.  
534 51408594), the State Key Laboratory for GeoMechanics and Deep Underground Engineering,  
535 China University of Mining & Technology/China University of Mining & Technology,  
536 Beijing (SKLGDUEK1909). The authors gratefully appreciate this support.

### 537 **References**

- 538 [1] L. Lim, C. Wade, Experimental fire tests of two-way concrete slabs, fire engineering  
539 research report 02/12, University of Canterbury and BRANZ Ltd, New Zealand, 2002.
- 540 [2] L. Lim, A. Buchanan, P. Moss, J.M. Franssen, Numerical modelling of two-way  
541 reinforced concrete slabs in fire, Eng. Struct. 26 (2004) 1081-1091.
- 542 [3] C.G. Bailey, W.S. Toh, Behaviour of concrete floor slabs at ambient and elevated  
543 temperatures, Fire Saf. J. 42 (2007) 425-436.
- 544 [4] C.G. Bailey, W.S. Toh, Small-scale concrete slab tests at ambient and elevated  
545 temperatures, Eng. Struct. 29 (2007) 2775-2791.
- 546 [5] L. Lim, A. Buchanan, P. Moss, J.M. Franssen, Computer modeling of restrained reinforced  
547 concrete slabs in fire conditions, J. Struct. Eng-ASCE. 130 (2004) 1964-1971.
- 548 [6] L.Z. Li, X. Liu, J.T. Yu, et al., Experimental study on seismic performance of post-fire  
549 reinforced concrete frames, Eng. Struct. 179 (2019) 161-173.
- 550 [7] Y.L. Dong, C.J. Zhu, Limit load carrying capacity of two-way slabs with two edges  
551 clamped and two edges simply supported in fire, J. Struct. Eng-ASCE. 137 (2010) 1182-  
552 1192.
- 553 [8] Y. Wang, G.L. Yuan, Z.H. Huang, et al, Experimental study on the fire behaviour of  
554 reinforced concrete slabs under combined in-plane and out-of-plane loads, Eng. Struct.

- 555 128 (2016) 316-332.
- 556 [9] Park, R. and Gamble, W.L. Reinforced Concrete Slabs, John Wiley & Sons Inc, Chichester,  
557 UK, 2000.
- 558 [10] Y. Wang, L A Bisby, T.Y. Wang, et al, Fire behaviour of reinforced concrete slabs under  
559 combined biaxial in-plane and out-of-plane loads, *Fire Saf. J.* 96 (2018) 27-45.
- 560 [11] Y. Wang, G.L. Yuan, Z.H. Huang, et al, Modelling of reinforced concrete slabs in fire,  
561 *Fire Saf. J.* 100 (2018) 171-185.
- 562 [12] H. Hajiloo, M.F. Green, Post-fire residual properties of GFRP reinforced concrete slabs:  
563 A holistic investigation, *Compos. Struct.* 201 (2018) 398-413.
- 564 [13] R. Van Coile, R. Caspeepele, L. Taerwe, Reliability-based evaluation of the inherent safety  
565 presumptions in common fire safety design, *Eng. Struct.* 77 (2014) 181-192.
- 566 [14] T. Molken, R. Van Coile, T. Gernay, Assessment of damage and residual load bearing  
567 capacity of a concrete slab after fire: Applied reliability-based methodology, *Eng. Struct.*  
568 150 (2017) 969-985.
- 569 [15] C.H. Chung, I.M. Cho Rong, J. Park, Structural test and analysis of RC slab after fire  
570 loading, *Nucl. Eng. Technol.* 45 (2013) 223-236.
- 571 [16] Y Wang., W.X. Guo, Z.H. Huang, et al, Analytical model for predicting the load –  
572 deflection curve of post-fire reinforced-concrete slab, *Fire Saf. J.* 101 (2018) 63-83.
- 573 [17] J.T. Yu, Experimental and theoretical research on damage assessment of reinforced  
574 concrete member after fire, Thesis, Tongji University, Shanghai, 2007 (in Chinese).
- 575 [18] X.M. Hou, W.Z. Zheng, Experiment and analysis on the mechanical performance of  
576 unbonded prestressed concrete continuous slab after elevated temperature, *J. Hunan*  
577 *Univ.* 37 (2010) 6-13 (in Chinese).
- 578 [19] W.Z. Zheng, X.M. Hou, W.H. Chen, Experiment and analysis on mechanical  
579 performance of prestressed concrete simply-supported slab after elevated temperature,  
580 *J. Harbin Inst. Technol.* 43 (2011) 8-13 (in Chinese).
- 581 [20] W.Y. Gao, K.X. Hu, J.G. Dai, et al, Repair of fire-damaged RC slabs with basalt fabric-  
582 reinforced shotcrete, *Constr. Build. Mater.* 185 (2018) 79-92.
- 583 [21] O. Gooranorimi, G. Claire, F.D. Caso, et al. Post-Fire Behavior of GFRP Bars and

584 GFRP-RC Slabs, *J. Mater. Civ. Eng. ASCE* 30 (2018) 04017296.

585 [22] C.G. Bailey, I.W. Burgess, R.J. Plank, Analyses of the effects of cooling and fire spread  
586 on steel-framed buildings, *Fire Saf. J.* 26 (1996) 273-293.

587 [23] J.S. Gottfried, G. Rein, Travelling fires for structural design-Part I: literature review, *Fire*  
588 *Saf. J.* 54 (2012) 74-85.

589 [24] E. Rackauskaite, P. Kotsovinos, A. Jeffers, G. Rein, Structural analysis of multi-storey  
590 steel frames exposed to travelling fires and traditional design fires, *Eng. Struct.* 150(2017)  
591 271-287.

592 [25] E. Rackauskaite, P. Kotsovinos, G. Rein, Structural response of a steel-frame building to  
593 horizontal and vertical travelling fires in multiple floors, *Fire Saf. J.* 91 (2017) 542-552.

594 [26] Y Wang, Z.X. Chen, Y.Q Jiang, et al. Residual properties of three-span continuous  
595 reinforced concrete slabs subjected to different compartment fires. *Eng. Struct.*, 2020,  
596 208: 110352.

597 [27] Y. Wang, Y.K. Duan, Y.J. Zhang, et al, Behaviour of continuous reinforced concrete floor  
598 slabs subjected to different compartment fires, *Eng. Struct.* 197(2019) 109445.

599 [28] G.Q. Li, S.X. Guo, H.S. Zhou, Modeling of membrane action in floor slabs subjected to  
600 fire, *Eng. Struct.* 29 (2007) 880-887.

601 [29] Y.L. Dong, Tensile membrane effects of concrete slabs in fire, *Mag. Concr. Res.* 62 (2010)  
602 497-505.

603 [30] E. Omer, B.A. Izzuddin, A.Y. Elghazouli, Failure of unrestrained lightly reinforced  
604 concrete slabs under fire - Part I: analytical models, *Eng. Struct.* 32 (2010) 2631-2646.

605 [31] E. Omer, B.A. Izzuddin, A.Y. Elghazouli, Failure of unrestrained lightly reinforced  
606 concrete slabs under fire - Part II: verification and application, *Eng. Struct.* 32 (2010)  
607 2647-2657.

608 [32] K.A. Cashell, A.Y. Elghazouli, B.A. Izzuddin, Failure assessment of lightly reinforced  
609 floor slabs. II: analytical studies, *J. Struct. Eng.* 137 (2011) 989-1001.

610 [33] B. Herraiz, T. Vogel, Novel design approach for the analysis of laterally unrestrained  
611 reinforced-concrete slabs considering membrane action, *Eng. Struct.* 123 (2016) 313-  
612 329.

- 613 [34] I. Burgess, Yield line plasticity and tensile membrane action in lightly-reinforced  
614 rectangular concrete slabs, *Eng. Struct.* 138 (2017) 195-214.
- 615 [35] GB 50010-2010 Code for Design of Concrete Structures, China Architecture and  
616 Building Press, Beijing, 2010 (in Chinese).
- 617 [36] Code for fire protection design of buildings (GB 50016-2014). Beijing; 2018 [in  
618 Chinese].
- 619 [37] GB/T 50152-1992 Standard for test method of concrete structures, China Architecture  
620 and Building Press, China, Beijing, 1992 (in Chinese).
- 621 [38] T Gernay. Fire resistance and burnout resistance of reinforced concrete columns. *Fire*  
622 *Saf. J.*, 104(2019) 67-78.
- 623 [39] T Gernay, J M Franssen. A performance indicator for structures under natural fire. *Eng.*  
624 *Struct.* 100 (2015) 94-103.
- 625 [40] J.C. Liu, K.H. Tan, Y. Yao, A new perspective on nature of fire-induced spalling in  
626 concrete, *Constr. Build. Mater.* 184 (2018) 581-590.
- 627 [41] X.L. An, Fire and Post-fire carrying capacity study of two-way restrained concrete slabs,  
628 Thesis, China University of Mining and Technology, 2017 (in Chinese).
- 629 [42] Antonio Marí, Antoni Cladera, Eva Oller , Jesús M. Bairán. A punching shear mechanical  
630 model for reinforced concrete flat slabs with and without shear reinforcement. *Eng.*  
631 *Struct.* 166 (2018) 413-426.
- 632 [43] Ala Torabian, Brisid Isufi, Davood Mostofinejad, António Pinho Ramos. Behaviour of  
633 thin lightly reinforced flat slabs under concentric loading. *Eng. Struct.* 196 (2019)  
634 109327.
- 635 [44] Xu Yang, Wan-Yang Gao, Jian-Guo Dai, Zhou-Dao Lu. Shear strengthening of RC  
636 beams with FRP grid-reinforced ECC matrix. *Compos. Struct.* 214 (2020) 112120.
- 637 [45] ACI Committee 318, Building code requirements for structural concrete and commentary.  
638 ACI 318-11, American Concrete Institute, Farmington Hills, 2011.
- 639 [46] EN 1994-1-1: Design of composite steel and concrete Structures-Part 1-1: General Rules  
640 and Rules for Buildings, CEN, Brussels, Belgium, 2007.
- 641 [47] Wu J. C. Experimental study on fire (post-fire) behaviours of concrete continuous two-



642 way slabs. Thesis, China University of Mining and Technology, China, 2020 (in  
643 Chinese).

644 [48] Z.Q. Wang, J. He, Nonlinear analysis of reinforced concrete structures, Harbin Institute  
645 of Technology Press, Harbin, 2016 (in Chinese).

646

647 **Figure Captions**

648 **Fig. 1.** Details of steel reinforcement layouts for the four slabs (all dimensions in mm) (a)  
649 Slabs B1, B2 and B3; (b) Slab B4; (c) Typical layout of thermocouples in the concrete  
650 slab; and (d) Thermocouples across the full-depth of each slab.

651 **Fig. 2** Details of the test setup (all dimensions in mm): (a) Photograph of the test setup; (b)  
652 Photograph of the support; (c) Plan view of the test setup; (d) Cross section 1-1 of test  
653 setup.

654 **Fig. 3** Details and instrument layout of four slabs (all dimensions in mm): (a) Layout of  
655 reinforcement and concrete strain gages; (b) Layout of displacement transducers.

656 **Fig. 4** Concrete temperature-time curves of the four slabs (the curves with broken line in the  
657 figure are the fire curves): (a) Slab B1; (b) Slab B2; (c) Slab B3; and (d) Slab B4.

658 **Fig. 5** Temperature-time curves of the reinforcing steels for the four slabs: (a) Slab B1; (b)  
659 Slab B2; (c) Slab B3; and (d) Slab B4.

660 **Fig. 6** Failure modes of Slab B1-PF (all dimensions in mm): (a) Photograph of cracks on the  
661 top surface; (b) Crack pattern on the top surface; (c) Photograph of cracks on the  
662 bottom surface; and (d) Crack pattern on the bottom surface.

663 **Fig. 7** Failure modes of Slab B2-PF (all dimensions in mm): (a) Photograph of cracks on the  
664 top surface; (b) Crack pattern on the top surface; (c) Photograph of cracks on the  
665 bottom surface; and (d) Crack pattern on the bottom surface.

666 **Fig. 8** Failure modes of Slab B3-PF (all dimensions in mm): (a) Photograph of cracks on the  
667 top surface; (b) Crack pattern on the top surface; (c) Photograph of cracks on the  
668 bottom surface; and (d) Crack pattern on the bottom surface.

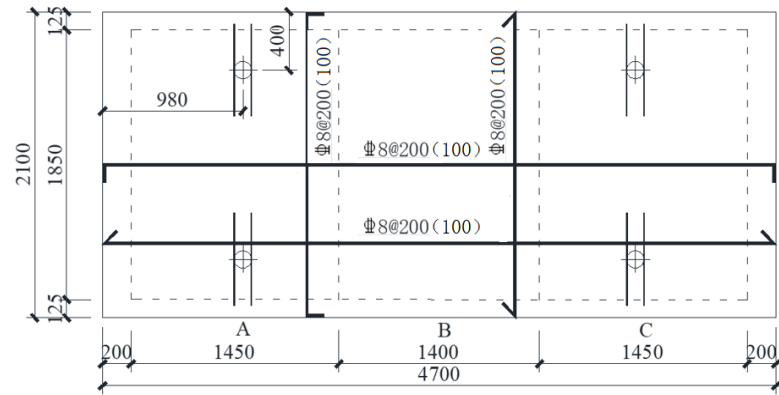
669 **Fig. 9** Failure modes of Slab B4-PF (all dimensions in mm): (a) Photograph of crack on the  
670 top surface; (b) Crack pattern on the top surface; (c) Photograph of cracks on the  
671 bottom surface; and (d) Crack pattern on the bottom surface.

672 **Fig. 10** Vertical deflection-load curves of four slabs: (a) Slab B1-PF; (b) Slab B2-PF; (c) Slab  
673 B3-PF; and (d) Slab B4-PF.

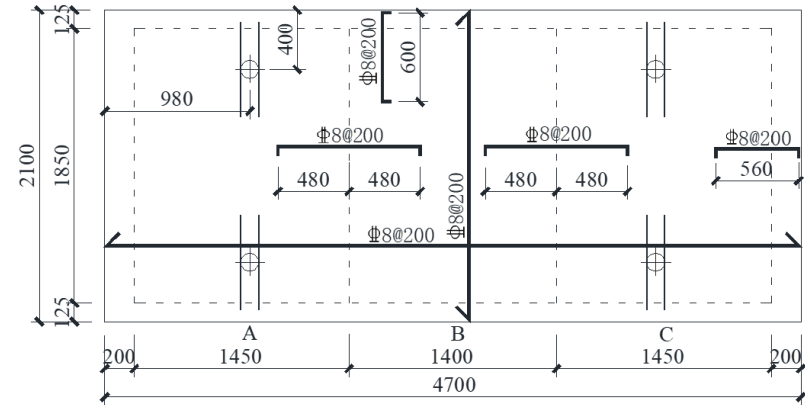
674 **Fig.11.** Ductility factor of absorption energy.

675 **Fig. 12** Horizontal deflection and restraint forces of tested slabs: (a) load-horizontal deflection  
676 curves of Slabs B1-PF and B2-PF; (b) restraint force-load curve of Slab B1-PF; and  
677 (c) restraint force-load curve of Slab B3-PF.

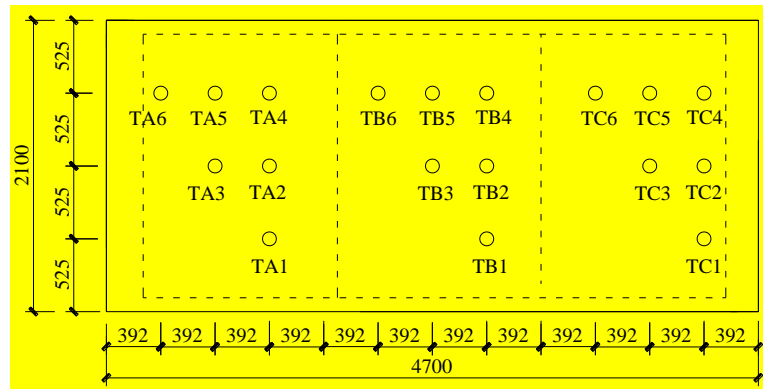
678 **Fig. 13** Concrete and reinforcement strain-load curves of four slabs: (a) Slab B1-PF; (b) Slab  
679 B2-PF; (c) Slab B3-PF; and (d) Slab B4-PF.



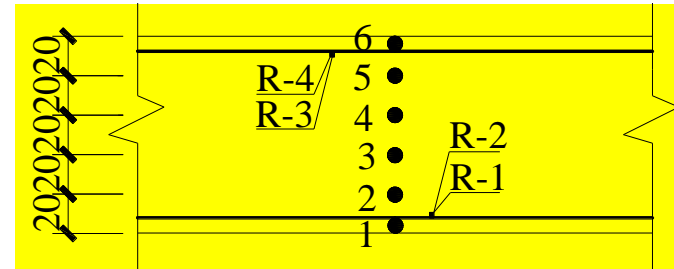
(a) Slabs B1 and B2 (B3)



(b) Slab B4



(c) Typical layout of thermocouples in the concrete slab



(d) Thermocouples across the full-depth of each slab

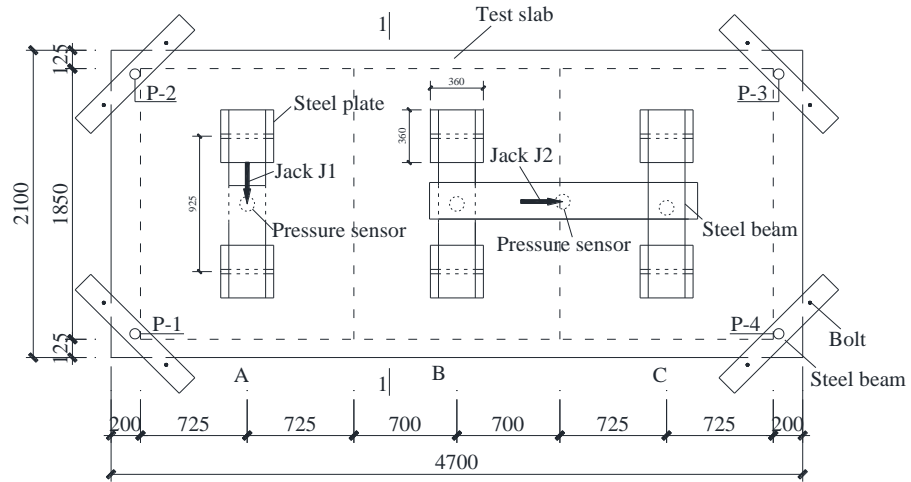
**Fig. 1.** Details of steel reinforcement layouts for the four slabs (all dimensions in mm) (a) Slabs B1, B2 and B3; (b) Slab B4; (c) Typical layout of thermocouples in the concrete slab; and (d) Thermocouples across the full-depth of each slab



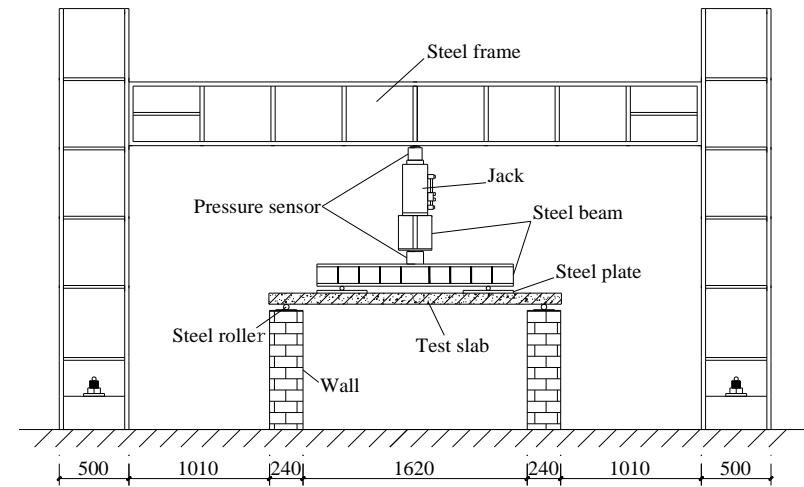
(a) Photograph of the test setup



(b) Photograph of the support

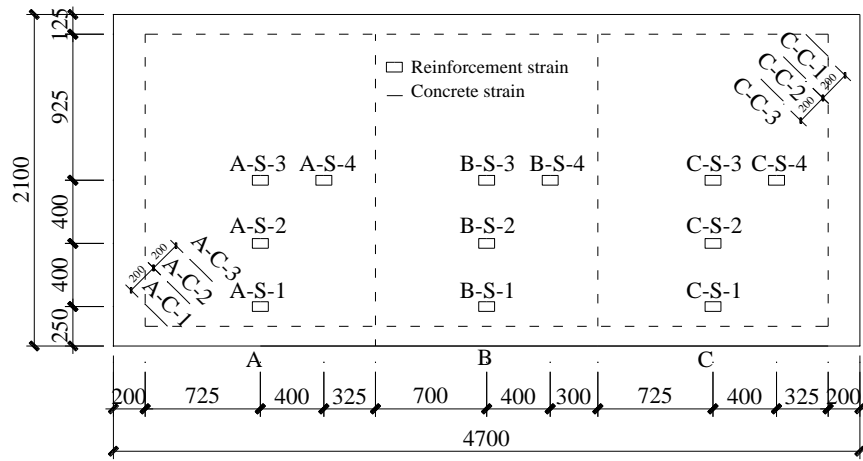


(c) Plan view

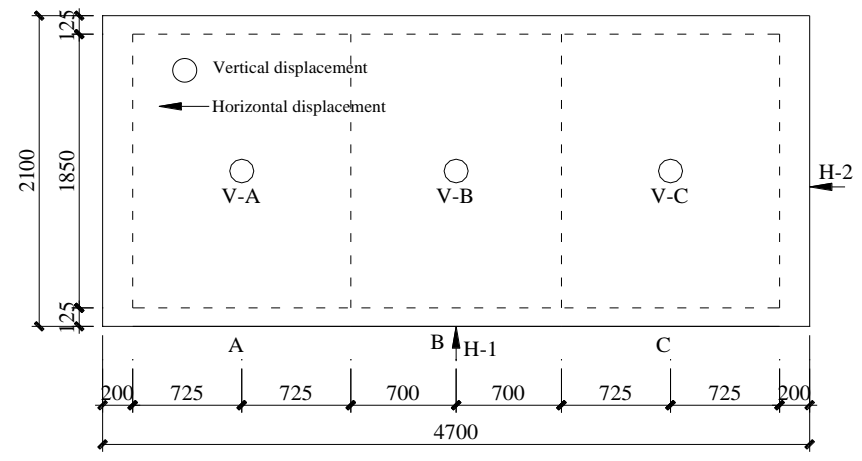


(d) Cross section 1-1

**Fig. 2.** Details of the test setup (all dimensions in mm): (a) Photograph of the test setup; (b) Photograph of the support; (c) Plan view of the test setup; (d) Cross section 1-1 of test setup

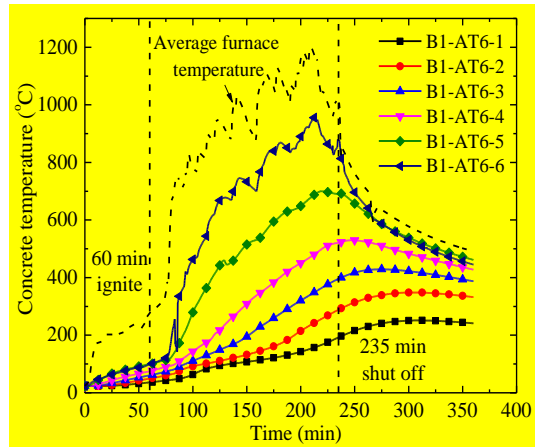


(a) Layout of reinforcement and concrete strain gages

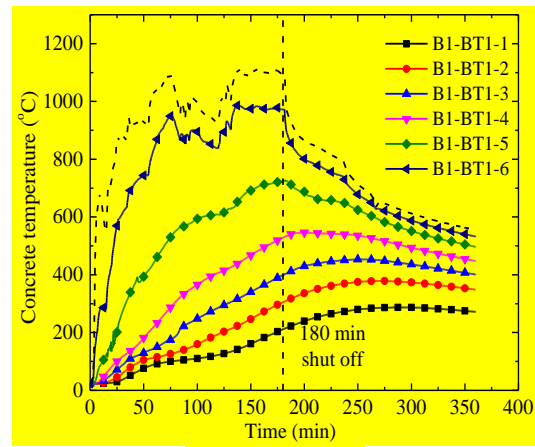


(b) Layout of displacement transducers

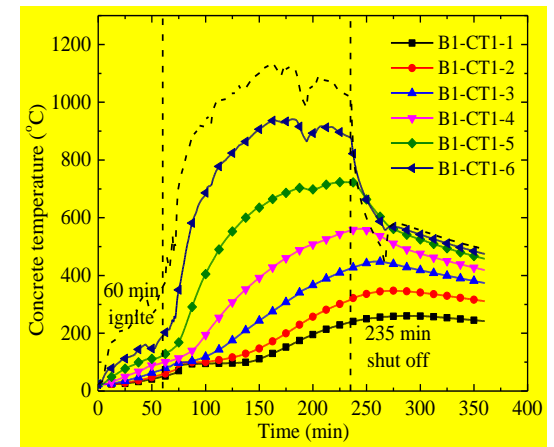
**Fig. 3.** Details and instrument layout of four slabs (all dimensions in mm): (a) Layout of reinforcement and concrete strain gages; (b) Layout of displacement transducers.



Compartment A

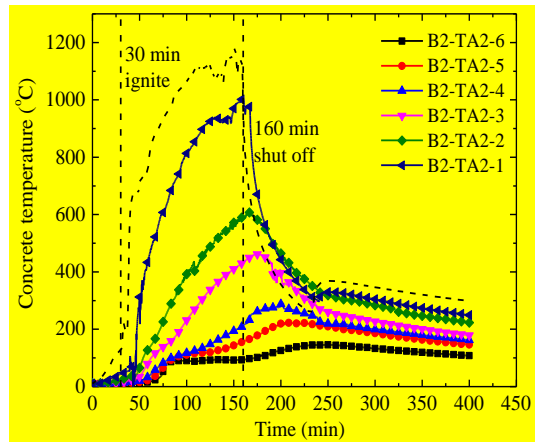


Compartment B

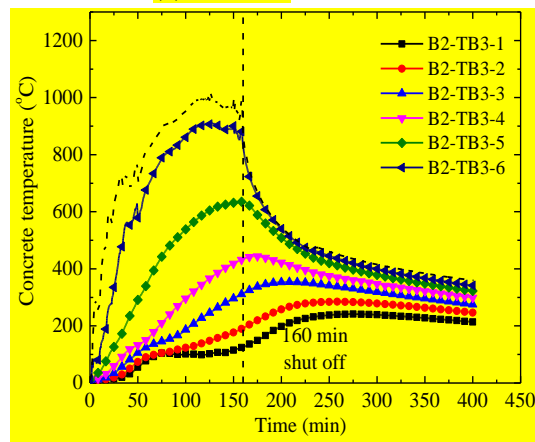


Compartment C

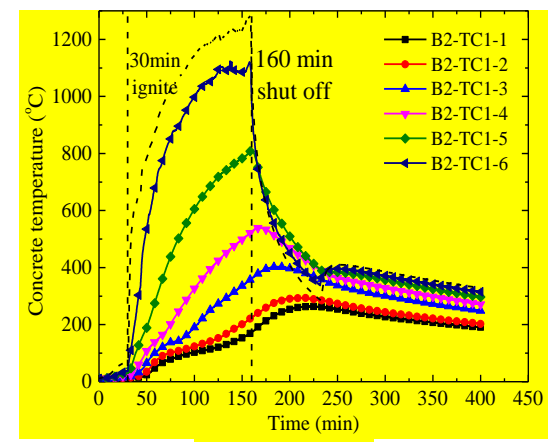
(a) Slab B1



Compartment A

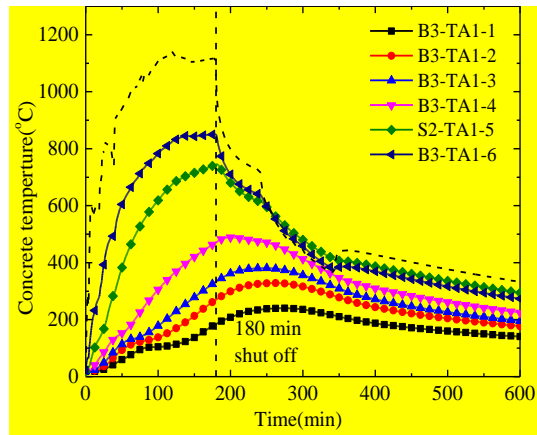


Compartment B

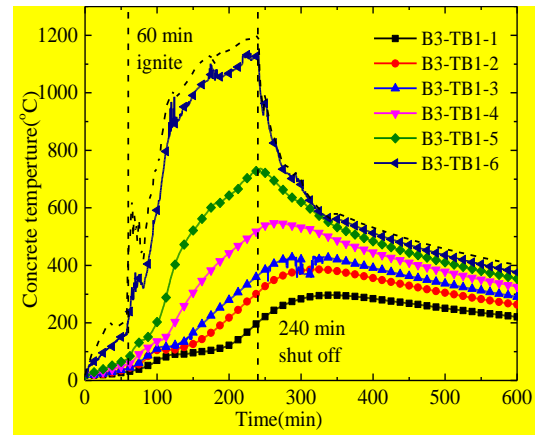


Compartment C

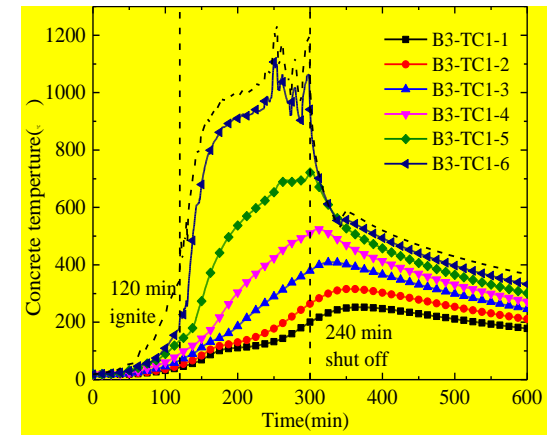
(b) Slab B2



Compartment A

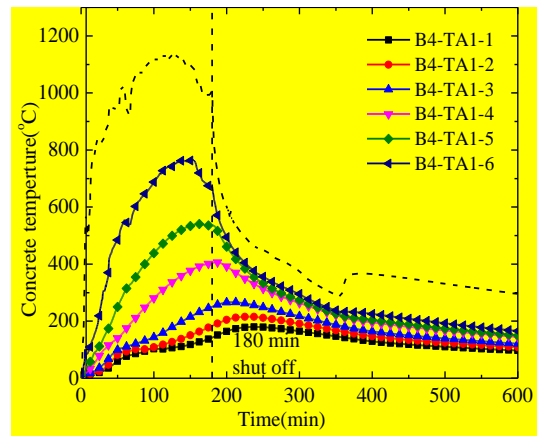


Compartment B

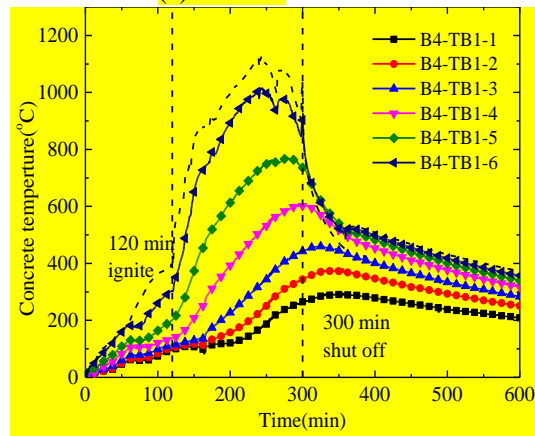


Compartment C

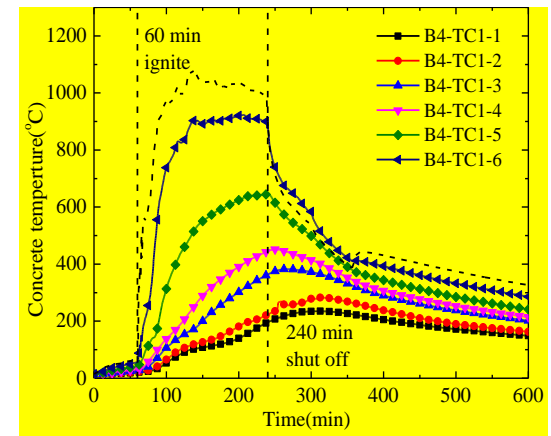
(c) Slab B3



Compartment A



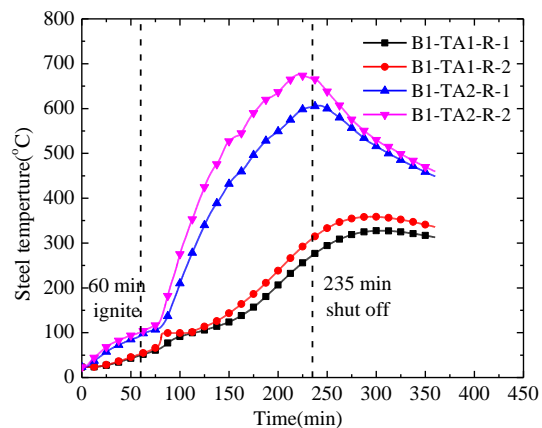
Compartment B



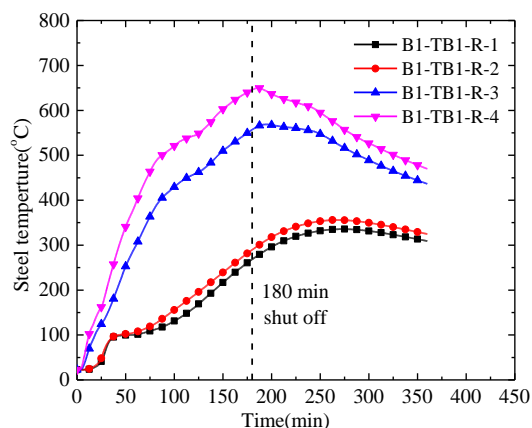
Compartment C

(d) Slab B4

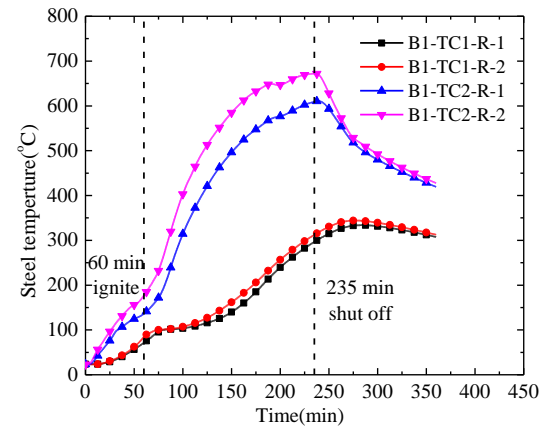
**Fig. 4.** Concrete temperature-time curves of the four slabs (the curves with broken line in the figure are the fire curves): (a) Slab B1; (b) Slab B2; (c) Slab B3; and (d) Slab B4



Compartment A

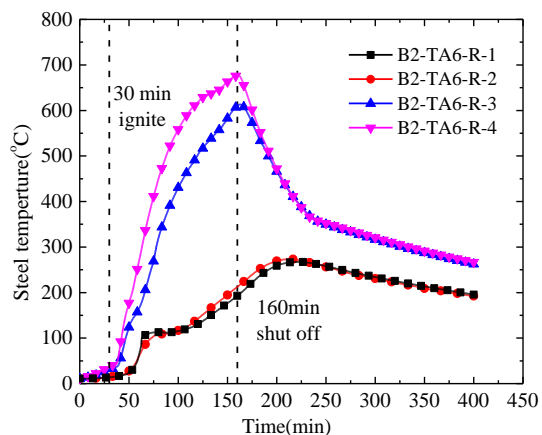


Compartment B

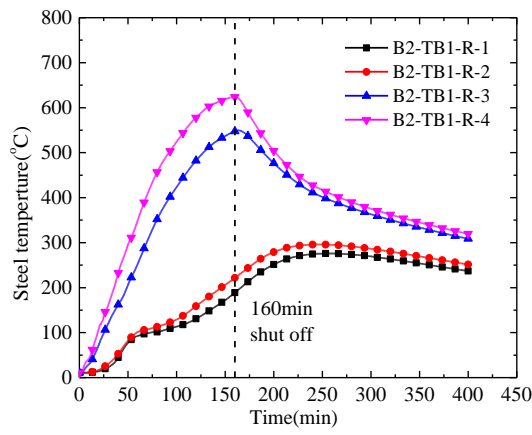


Compartment C

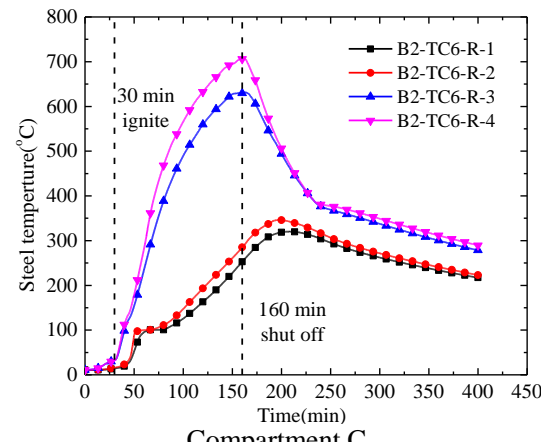
(a) Slab B1



Compartment A



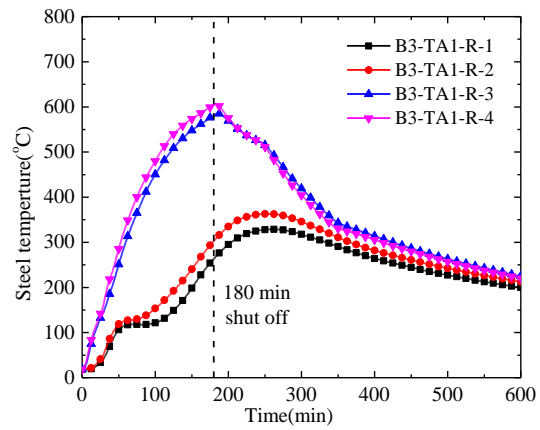
Compartment B



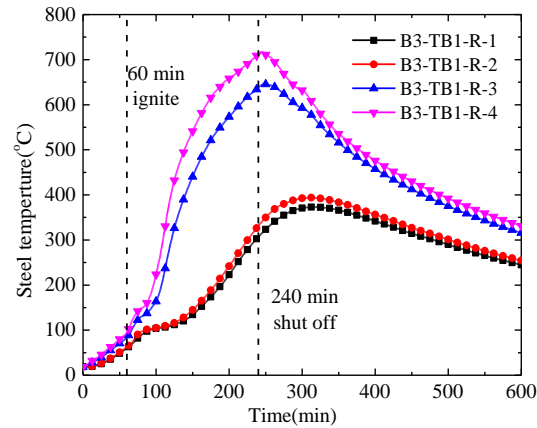
Compartment C

(b) Slab B2

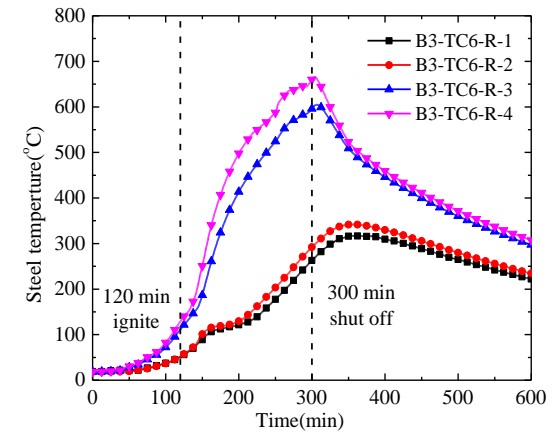




Compartment A

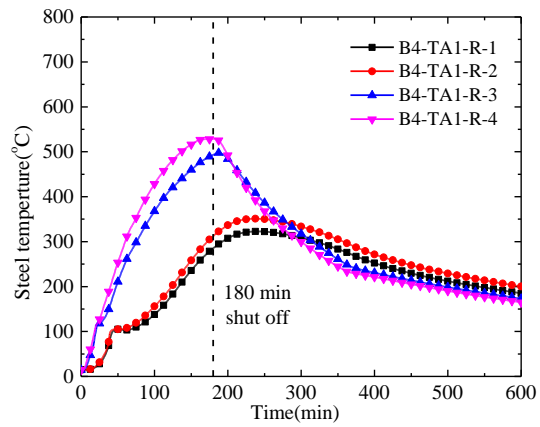


Compartment B

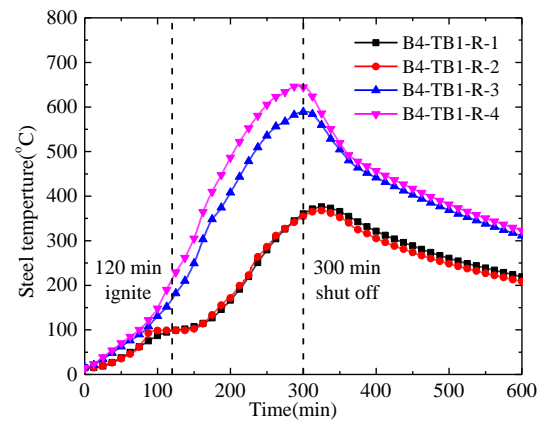


Compartment C

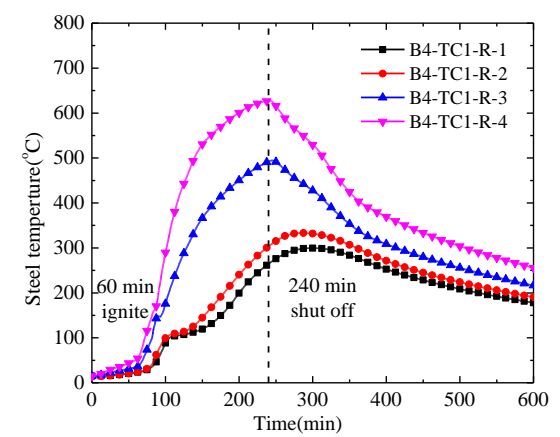
(c) Slab B3



Compartment A



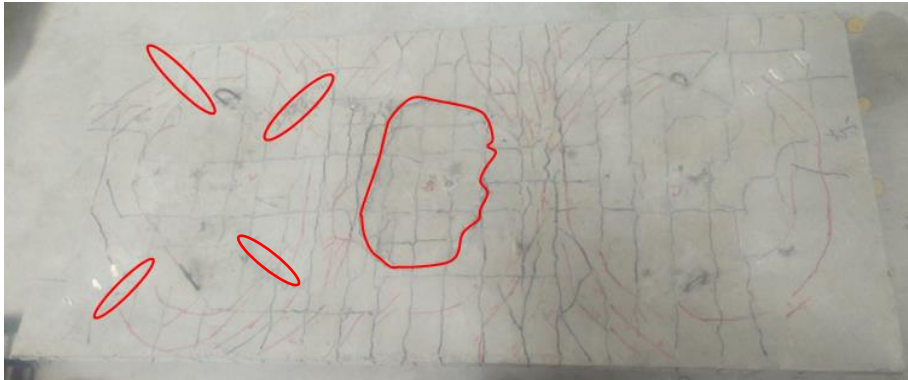
Compartment B



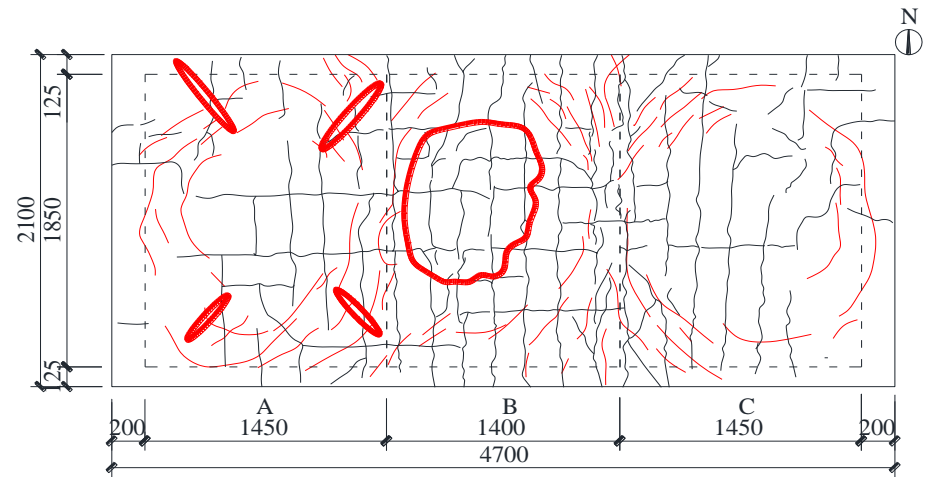
Compartment C

(d) Slab B4

**Fig. 5** Temperature-time curves of the reinforcing steels for the four slabs: (a) Slab B1; (b) Slab B2; (c) Slab B3; and (d) Slab B4.



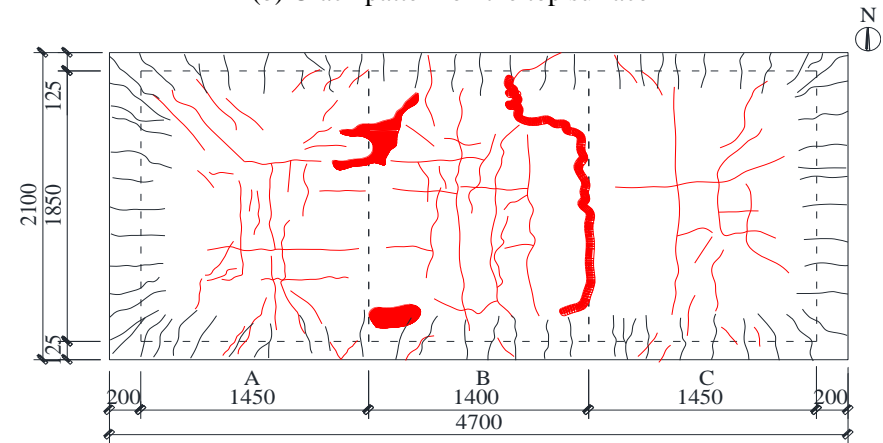
(a) Photograph of cracks on the top surface



(b) Crack pattern on the top surface



(c) Photograph of cracks on the bottom surface

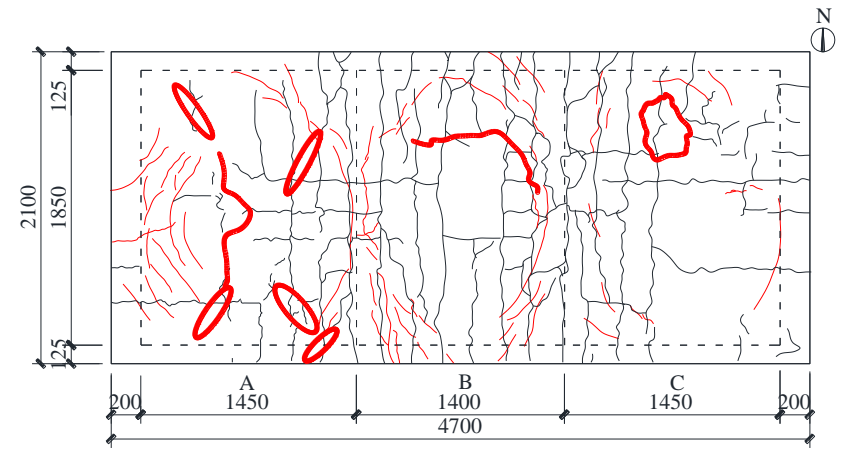


(d) Crack pattern on the bottom surface

**Fig. 6** Failure modes of Slab B1-PF (all dimensions in mm): (a) Photograph of cracks on the top surface; (b) Crack pattern on the top surface; (c) Photograph of cracks on the bottom surface; and (d) Crack pattern on the bottom surface



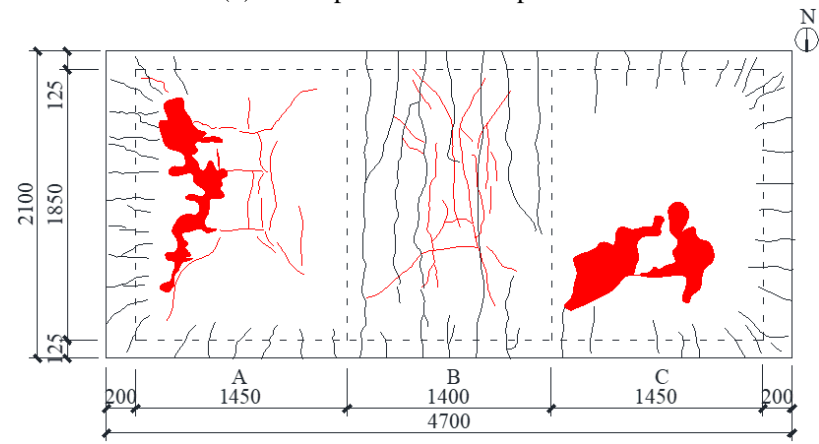
(a) Photograph of cracks on the top surface



(b) Crack pattern on the top surface

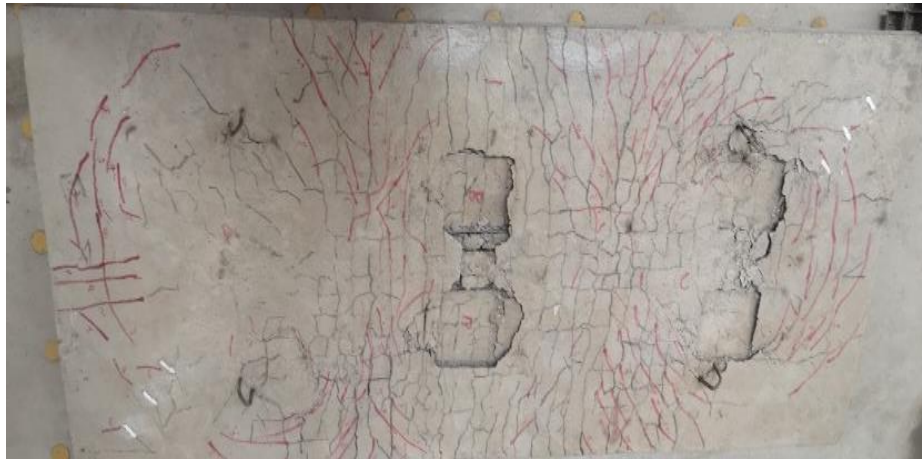


(c) Photograph of cracks on the bottom surface

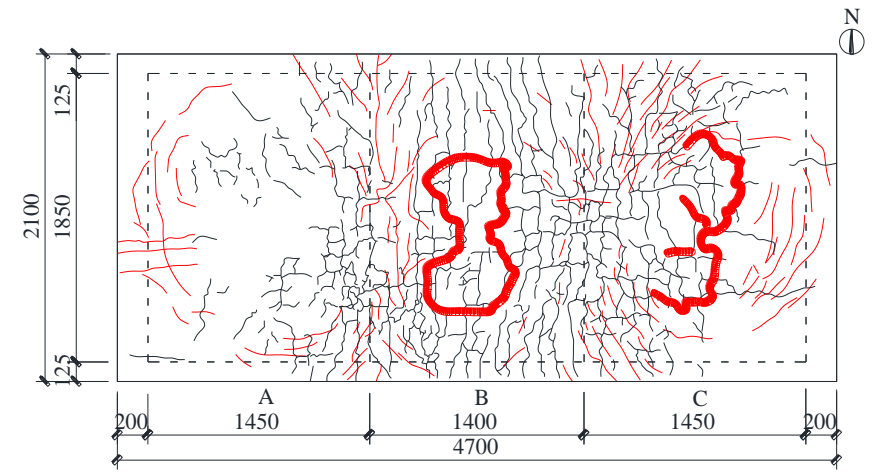


(d) Crack pattern on the bottom surface

**Fig. 7** Failure modes of Slab B2-PF (all dimensions in mm): (a) Photograph of cracks on the top surface; (b) Crack pattern on the top surface; (c) Photograph of cracks on the bottom surface; and (d) Crack pattern on the bottom surface



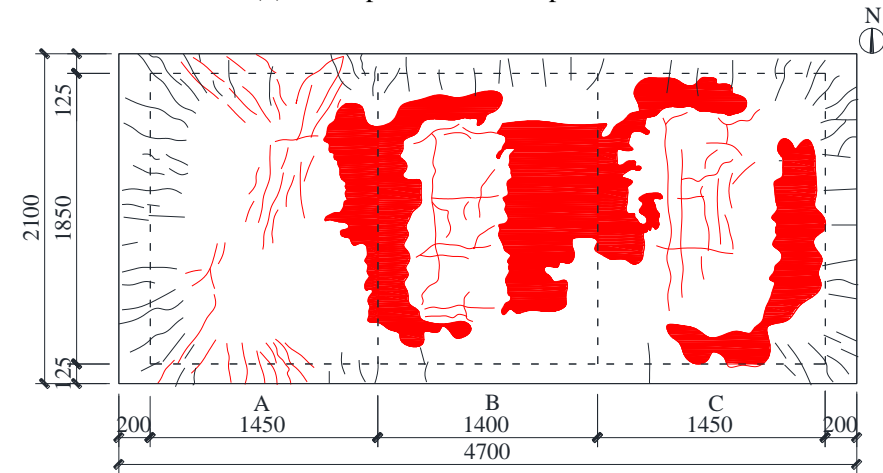
(a) Photograph of cracks on the top surface



(b) Crack pattern on the top surface



(c) Photograph of cracks on the bottom surface



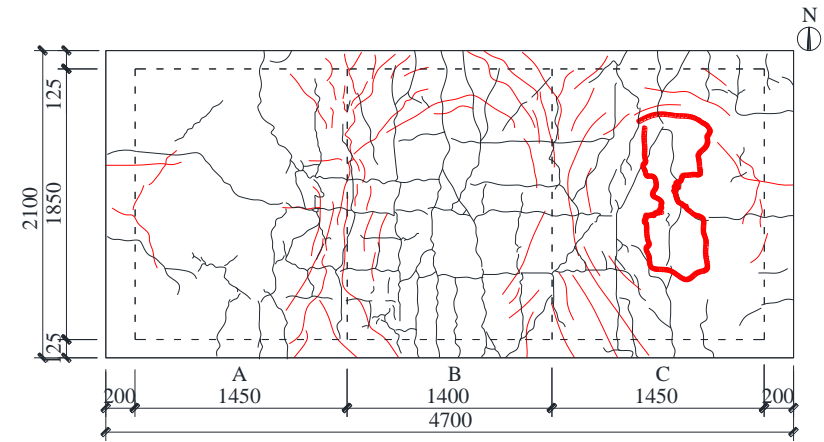
(d) Crack pattern on the bottom surface

**Fig. 8** Failure modes of Slab B3-PF (all dimensions in mm): (a) Photograph of cracks on the top surface; (b) Crack pattern on the top surface; (c) Photograph of cracks on the bottom surface; and (d) Crack pattern on the bottom surface





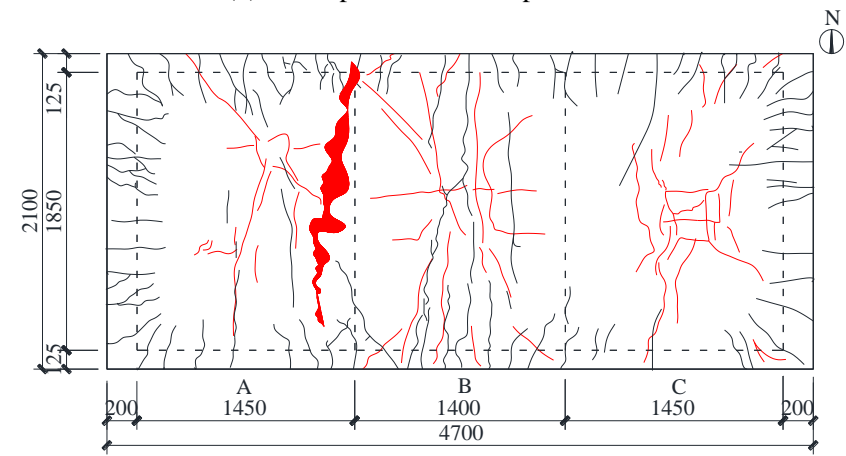
(a) Photograph of cracks on the top surface



(b) Crack pattern on the top surface

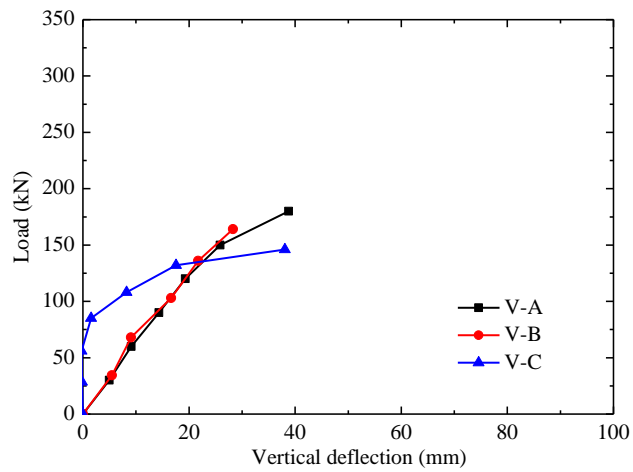


(c) Photograph of cracks on the bottom surface

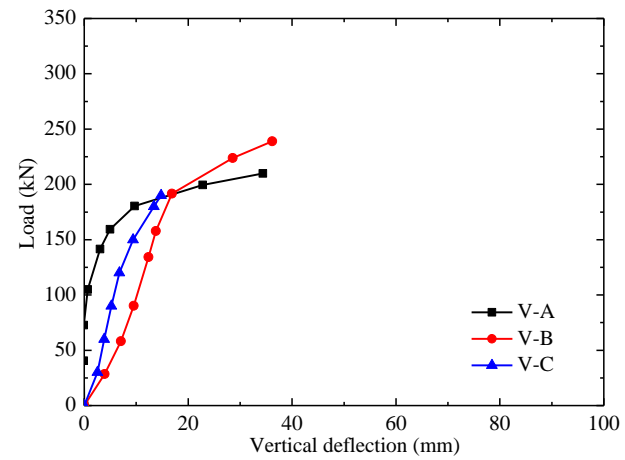


(d) Crack pattern on the bottom surface

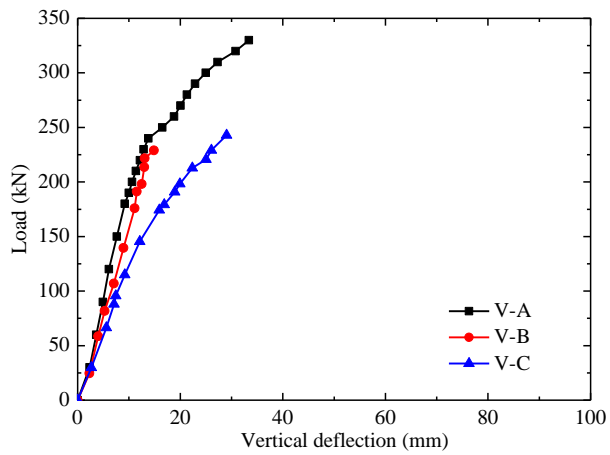
**Fig. 9** Failure modes of Slab B4-PF (all dimensions in mm): (a) Photograph of crack on the top surface; (b) Crack pattern on the top surface; (c) Photograph of cracks on the bottom surface; and (d) Crack pattern on the bottom surface



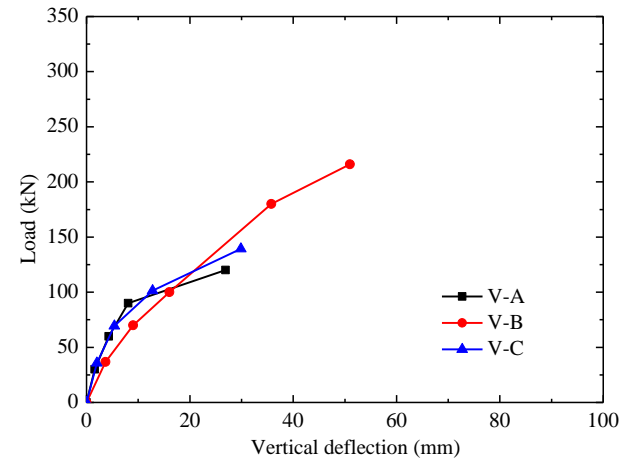
(a) Slab B1-PF



(b) Slab B2-PF



(c) Slab B3-PF



(d) Slab B4-PF

**Fig. 10** Vertical deflection-load curves of four slabs: (a) Slab B1-PF; (b) Slab B2-PF; (c) Slab B3-PF; and (d) Slab B4-PF

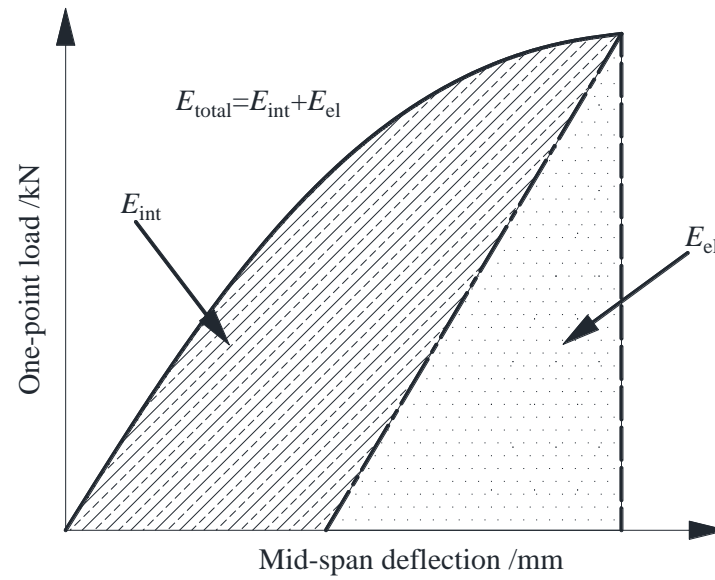
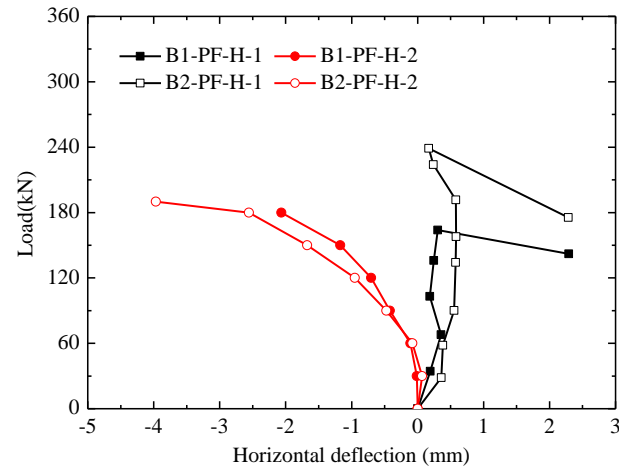
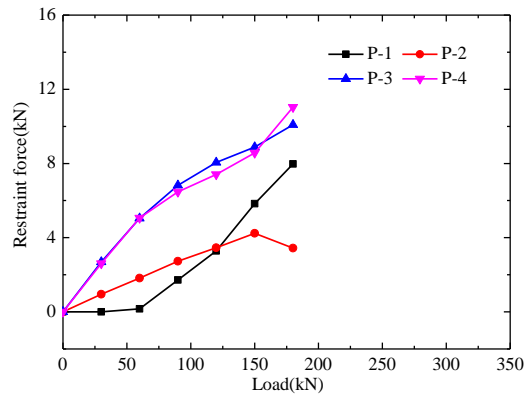


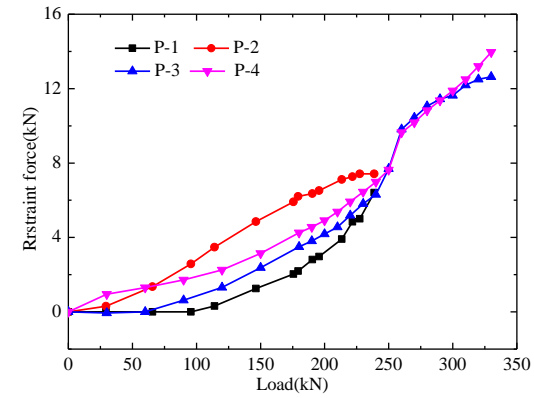
**Fig.11.** Ductility factor of absorption energy



(a) Load-horizontal deflection curves of Slabs B1-PF and B2-PF



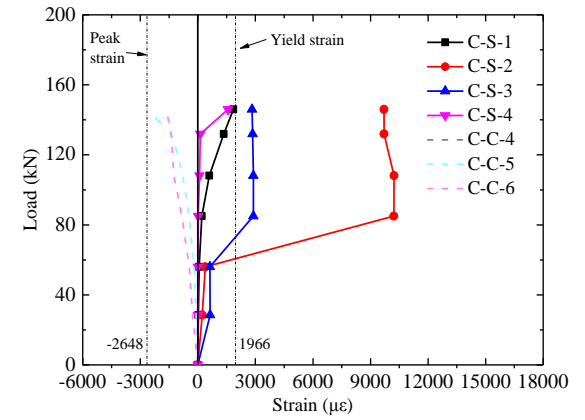
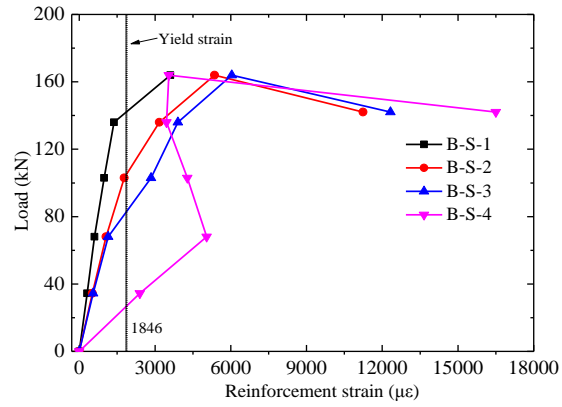
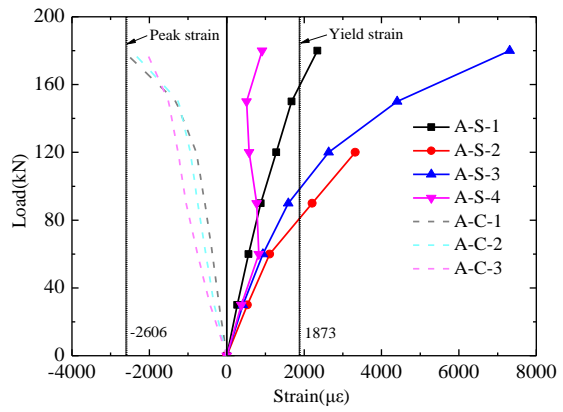
(b) Slab B1-PF



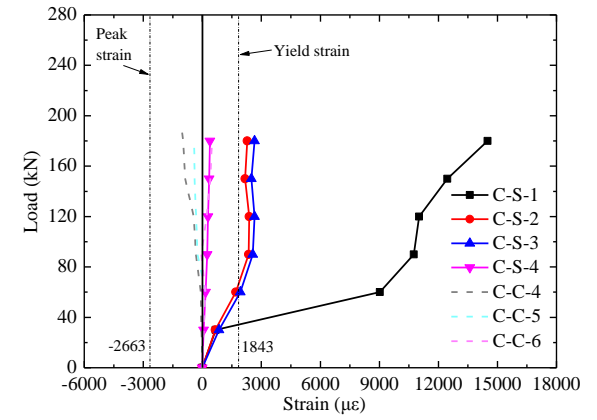
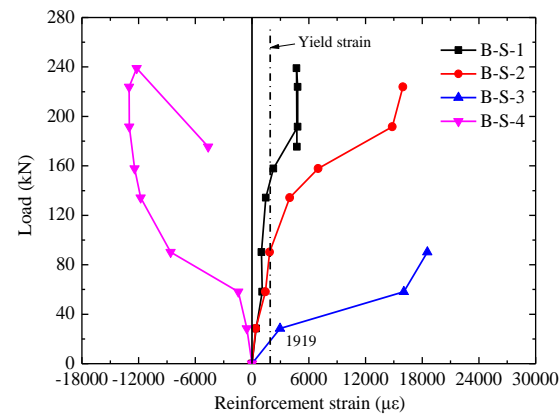
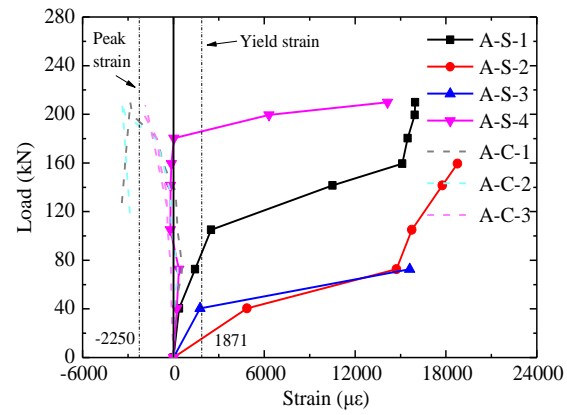
(c) Slab B3-PF

**Fig. 12** Horizontal deflection and restraint forces of tested slabs: (a) load-horizontal deflection curves of Slabs B1-PF and B2-PF; (b) restraint force-load curve of Slab B1-PF; and (c) restraint force-load curve of Slab B3-PF.

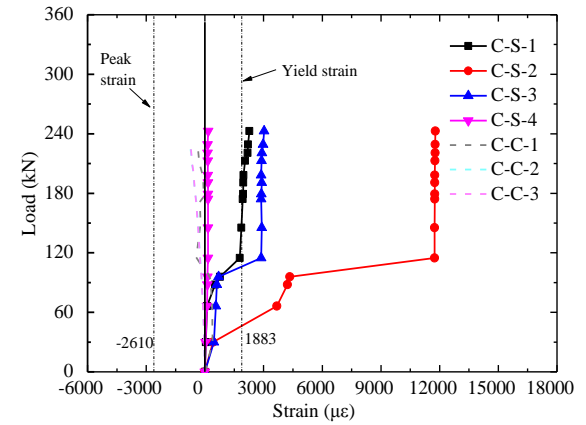
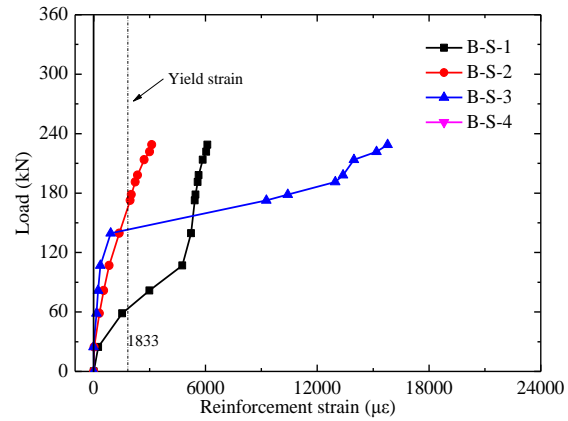
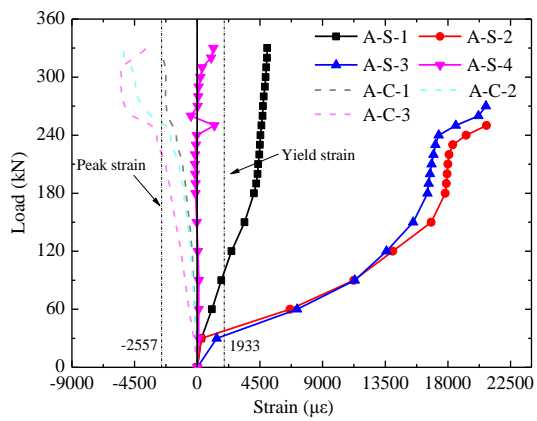




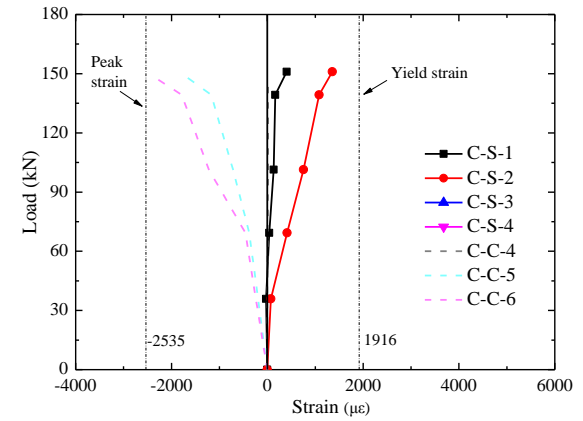
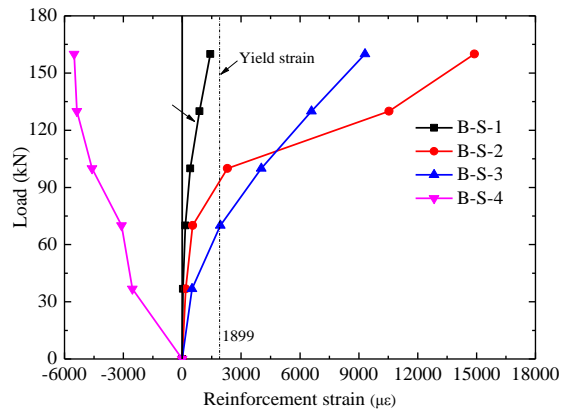
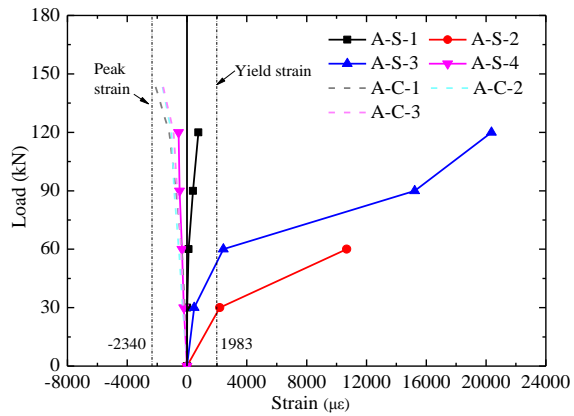
(a) Slab B1-PF



(b) Slab B2-PF



(c) Slab B3-PF



(d) Slab B4-PF

**Fig. 13** Concrete and reinforcement strain-load curves of four slabs: (a) Slab B1-PF; (b) Slab B2-PF; (c) Slab B3-PF; and (d) Slab B4-PF



[Click here to access/download](#)

**Table**

Tables-R1.docx



**Declaration of interests**

The authors declare that they have no known competing financial interests or personal relationships that could have appeared to influence the work reported in this paper.

The authors declare the following financial interests/personal relationships which may be considered as potential competing interests:

**Yong Wang:** Conceptualization, Methodology, Formal analysis, Investigation, Writing- Original draft preparation.

**Yaqiang Jiang:** Investigation, Data curation.

**Zhaohui Huang:** Supervision, Methodology, Writing - Review & Editing

**Lingzhi Li:** Validation

**Yuner Huang:** Validation

**Yajun Zhang:** Formal analysis

**Gengyuan Zhang:** Validation

**Xiaoyue Zhang:** Investigation

**Yakun Duan:** Data curation